Friction https://mc03.manuscriptcentral.com/friction
https://doi.org/10.26599/FRICT.2026.9441332

Review Article

Frictional heat in polymer tribological materials: Generation, characterization, degradation and regulation

Dezhi Teng[1], Jingsi Wang[1]✉, Xiaoxia Sa[2], Jiaqi Zhu[3] Pay Jun Liew[4]

[1]Marine Engineering College, Dalian Maritime University, 1 Linghai Road, Ganjingzi District, Dalian 116026, China

[2]Grikin Advanced Materials (Shandong) Co., Ltd., 6596 Dongfang Hong East Road, Yuanqiao Town, Economic and Technological Development Zone, Dezhou 253000, China

[3]Mechanical Engineering College, Tohoku University, Aoba Ku, Aramaki Aoba 6-6-01, Sendai, Miyagi 9808579, Japan

[4]Fakulti Teknologi Dan Kejuruteraan Industri Dan Pembuatan, Universiti Teknikal Malaysia Melaka, Hang Tuah Jaya, Melaka, Durian Tunggal 76100, Malaysia

✉ Corresponding author. E-mail: wjs@dlmu.edu.cn

Received: July 14, 2026; Revised: September 26, 2026; Accepted: October 29, 2026

© The Author(s) 2026.

Just Accepted

Abstract: Polymer composites are widely used in tribological systems owing to their low density, self-lubricating capability, and corrosion resistance. However, their intrinsically low thermal conductivity promotes frictional heat accumulation at the sliding interface, making frictional heat a critical factor influencing interfacial evolution, tribological performance, and service reliability. Rather than focusing solely on frictional heat as a temperature rise, this review considers the role in

the evolution of friction interfaces. The discussion covers heat generation mechanisms, analytical, numerical, and experimental approaches for temperature evaluation, thermally induced material and interfacial changes, and degradation caused by excessive heat accumulation. Thermal management strategies are summarized in terms of intrinsic thermal stability, friction reduction, heat dissipation, and interfacial regulation. Remaining challenges in quantitative heat source identification, criteria for beneficial and detrimental thermal effects, and engineering translation are also discussed to support thermal management and material design.

Keywords: Polymer, Tribology, Frictional heat, Thermal management

Just Accepted

1 Introduction

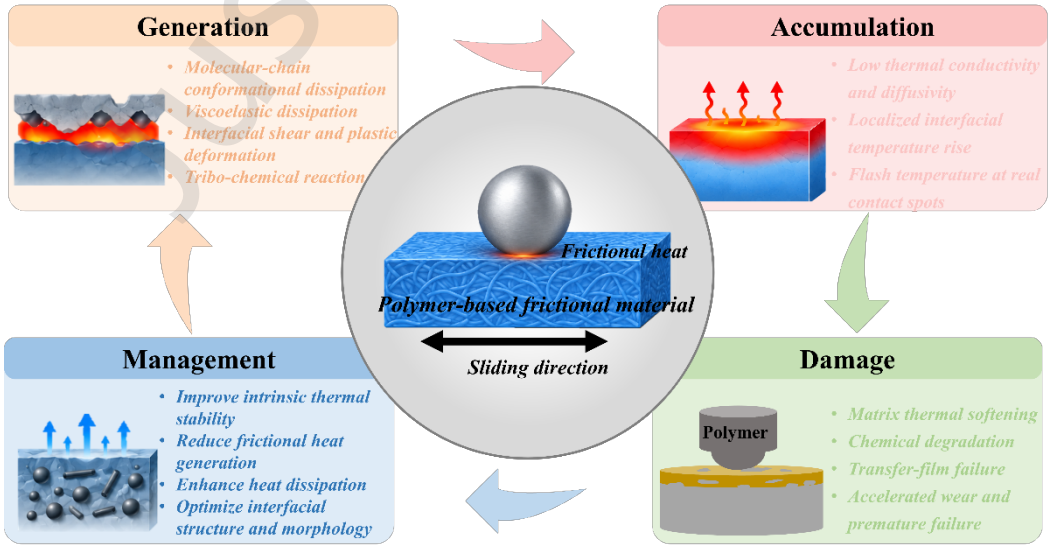
Polymers and their composites are widely used in tribological components, including bearings [1], gears [2], seals [3], and braking systems [4], because of their low density, excellent self-lubricating properties, corrosion resistance, and effective vibration and noise damping. However, increasing applied loads and sliding velocities generate substantial frictional heat at the contact interface, making frictional heat a key factor affecting the performance and service life of polymer tribological materials [5]. Unlike metals, where heat is primarily conducted by free electrons, heat transfer in polymers mainly relies on phonon transport [6]. The disordered molecular structure, high amorphous fraction, and strong phonon scattering give polymers intrinsically low thermal conductivity compared with metals. Tab. 1 summarizes the thermal conductivity of representative polymer materials. Limited heat dissipation promotes localized heat accumulation during sliding, which can alter the modulus, hardness, load bearing capacity, molecular mobility, and interfacial state of the polymer [7][8][9].

Tab. 1 Thermal conductivity of typical polymers.

Polymer	Thermal conductivity (W/(m·K))	Reference
PA	0.28	[10]

PPS	0.22	[11]
Epoxy	0.08-0.11	[12][13]
PEEK	0.28	[14]
PI	0.15	[15]
PAEK	0.18	[16]
UHMWPE	0.34	[17]
PTFE	0.33	[18]

Previous studies on polymer tribology have mainly examined frictional heating through interfacial temperature evolution and the associated changes in friction and wear [19][20][21]. A recent comprehensive review of polymer tribology has further identified thermal effects and localized melting as important mechanisms governing friction and wear, noting that frictional heating can alter rheological properties, reduce elastic modulus, and even induce surface layer melting [22]. These studies establish the importance of thermal effects in polymer tribology, while also indicating the need for a more focused consideration of frictional heat throughout the sliding process. Accordingly, as shown in Fig. 1, this review examines the mechanisms of frictional heat generation, methods for calculating and characterizing friction induced temperature, thermally induced changes and degradation of polymer materials and friction interfaces, and strategies for thermal management. By integrating these aspects with frictional heat as the organizing theme, the review aims to clarify the role of frictional heat in polymer tribological systems and to provide guidance for thermal management and material design.



Just Accepted

Fig. 1 Integrated framework of frictional heat generation, accumulation, damage, and management in polymer tribological materials.

2 Mechanisms of frictional heat generation

During friction, the input mechanical work is inevitably converted into heat. Frictional heat is therefore a direct result of energy dissipation across multiple scales. In all tribological systems, interfacial shear is the initial stage of mechanical energy input and dissipation. When two surfaces slide against each other, mechanical work is required to overcome frictional resistance. At real contact areas, asperities undergo adhesion, shearing, ploughing, and fracture, thereby directly converting mechanical energy into thermal energy [23]. Unlike metals, polymers possess long chain molecular structures, pronounced viscoelasticity, and low thermal conductivity. As a result, the mechanical energy input at the interface is not immediately and fully released as heat. Instead, it is first redistributed through internal structural evolution and then dissipated into heat via multiple physical mechanisms. This process mainly involves energy dissipation pathways across different scales, including molecular chain conformational relaxation, segmental viscoelastic response, and localized plastic deformation.

From a microscopic perspective, under sustained frictional shear, external mechanical work first induces internal rotation of the polymer backbone. This causes dihedral angles to deviate from their intrinsic equilibrium conformations. As a result, mechanical energy is temporarily stored within the molecular chains as conformational potential energy, primarily in the form of dihedral potential energy. However, this deformation is not static. The molecular chains undergo aperiodic stretch relaxation fluctuations in the shear flow field. This non-equilibrium dynamic process gradually releases the stored conformational potential energy. The released energy is then directly converted into kinetic energy of the system through segmental thermal motion. Macroscopically, this process manifests as continuous and irreversible frictional heat generation. Owing to differences in chain stiffness, the aperiodic conformational fluctuation behaviors vary significantly, leading to markedly

Just Accepted

different heat generation characteristics. As shown in Fig. 2 (a), for soft molecular chains such as PTFE, aperiodic stretch relaxation fluctuations persist during the steady friction stage (1-10 ns). These fluctuations drive continuous conversion between potential and kinetic energy, thereby maintaining a pronounced temperature rise in the system. As shown in Fig. 2 (b), for molecular chains with higher stiffness such as PI, only limited conformational rearrangement occurs during the initial friction stage (1-4 ns). The radius of gyration distribution then rapidly stabilizes. In the slip region, the chains almost cease to exhibit fluctuations after 4 ns, which interrupts the conversion between potential and kinetic energy. Consequently, the temperature rise essentially stops after 4 ns, and the overall temperature increase is significantly lower than that of PTFE [24].

Recent molecular dynamics studies have further revealed the diversity in the spatial dissipation modes of this mechanism [25]. As shown in Fig. 2 (c), POM achieves conformational dissipation primarily through changes in bond angles *and* dihedral angles. This dissipative behavior extends several nanometers into the subsurface, exhibiting a dissipation pattern distributed across the entire thickness direction. The dissipation of PTFE relies mainly on the reorganization of non-bonded interactions near the interface. This results in a dissipation pattern localized in the near interface region, accompanied by a distinct subsurface temperature rise peak. These results indicate that the generation of frictional heat in polymers is not only governed by chain stiffness but is also closely related to the chemical structure of the molecular chains and the nature of intermolecular interactions.

The conformational dissipation described above essentially represents energy conversion through conformational changes of polymer chains under frictional shear. For polymer systems with pronounced viscoelasticity, such as natural rubber, styrene butadiene rubber, and polyurethane elastomers, the frictional heat originates primarily from viscoelastic dissipation caused by internal friction during segmental motion. This type of dissipation can be classified into two categories. The first is hysteresis loss, which refers to the irreversible energy dissipation caused by internal friction between segments during cyclic compression-rebound deformation [26]. The second is interface-

Just Accepted

induced viscoelastic frictional dissipation, which arises from localized high frequency micro-vibrations induced by surface roughness [27][28]. These micro-vibrations cause a time dependent viscoelastic response of the polymer and convert mechanical energy into heat. A study has shown that in water-lubricated rubber bearings, even under hydrodynamic lubrication conditions, the contribution of fluid shear is limited due to the extremely low viscosity of water. As shown in Fig. 2(d), the contribution of viscoelastic dissipation to the transient friction coefficient and total heat flux still exceeds that of actual contact shear and fluid shear [29]. This indicates that for rubber components operating in mixed lubrication regimes, controlling the viscoelastic response of the material is an important approach to reducing frictional heat accumulation.

The viscoelastic response involved in this dissipation process is strongly dependent on both temperature and deformation frequency. For polymers that approximately obey the time-temperature superposition (TTS) principle, changes in temperature can be related to equivalent changes in deformation frequency, allowing dynamic mechanical behavior over a broad temperature and frequency range to be represented by a master curve. The Williams-Landel-Ferry (WLF) relation is commonly used to describe this temperature dependent shift near the glass transition region [30]. In sliding contacts, repeated deformation caused by surface asperities introduces characteristic deformation frequencies related to sliding velocity and surface roughness. TTS therefore provides a useful framework for relating the local thermal state and deformation frequency to dynamic mechanical properties such as the loss modulus and loss factor, which characterize viscoelastic energy dissipation [28][31]. This temperature and frequency dependence should be considered when evaluating frictional heat generation and when selecting material properties and operating conditions to avoid regimes of excessive viscoelastic loss. However, TTS mainly describes the viscoelastic contribution to frictional heating. Under more complex frictional conditions, nonlinear deformation, interfacial slip, structural evolution, and tribo-chemical reactions may also contribute to the overall energy dissipation.

Just Accepted

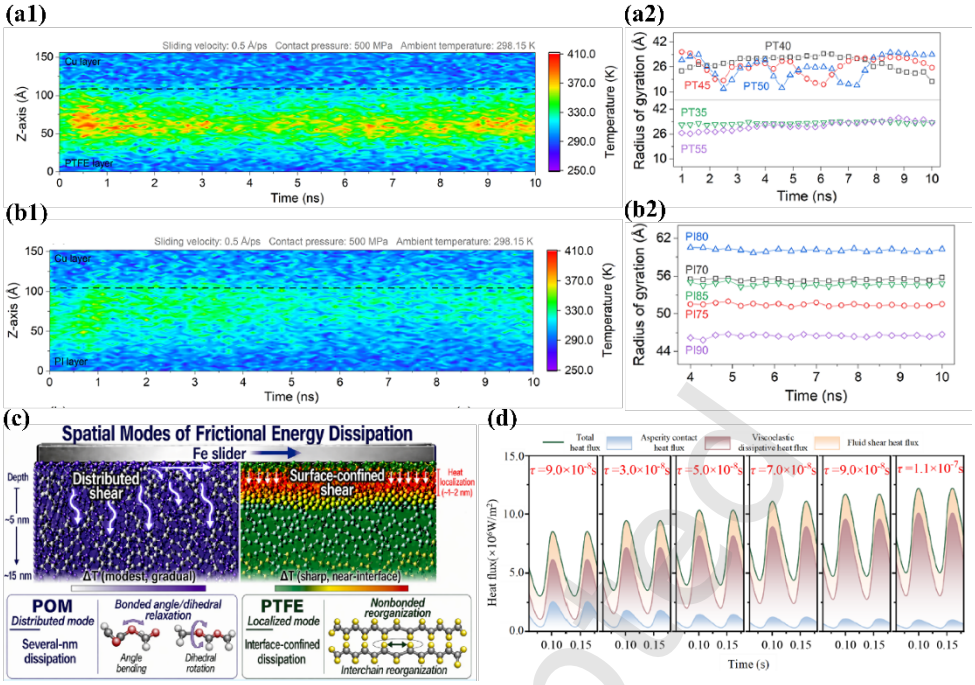


Fig. 2 Representative frictional heat generation mechanisms in polymers. (a) Temperature evolution and representative molecular chain fluctuation of PTFE during sliding; (b) temperature evolution and conformational stabilization of PI during sliding [24]; (c) contrasting spatial energy dissipation modes in POM and PTFE [25]; (d) contributions of viscoelastic deformation, asperity contact, and fluid shear to heat generation in a water lubricated rubber bearing [29].

Additionally, during the running-in stage or under conditions of high load and high surface roughness, local plastic deformation is also an important internal dissipation mechanism. Within the real contact area, the material undergoes irreversible deformation such as yielding, plastic flow, abrasive micro-cutting, and fatigue spalling. These processes convert mechanical energy into heat through plastic dissipation [32]. Compared with metallic materials, plastic deformation in polymers typically occurs together with segmental orientation, disentanglement, and thermal softening. Therefore, their heat generation behavior exhibits more pronounced time dependence and structural sensitivity.

When the sliding speed, contact pressure, or interface temperature increases further, tribo-chemical reactions gradually become a non-negligible additional heat source. Under friction, polymers may undergo chain scission, crosslinking, oxidation, and free-radical reactions, with associated heat release. For example, PEEK undergoes chain scission and oxidation during high-temperature sliding [33], and the formation of oxide films on steel/polymer tribo-pairs is an

Just Accepted

exothermic process [23]. Although tribo-chemical heat is usually not the primary source of frictional heat, under conditions of high flash temperatures or prolonged service, its continuous accumulation can further alter the material structure and interface state. This, in turn, feeds back to affect subsequent frictional heat generation and interfacial temperature rise.

The above molecular-scale and microscopic interfacial mechanisms reveal the intrinsic origins of frictional heat generation. These mechanisms are not mutually exclusive. Instead, frictional heating in polymer tribological systems generally results from their combined contributions. Owing to differences in molecular architecture, viscoelastic behavior, crystallinity, thermal stability, and interfacial chemistry, the predominant heat-generation pathway varies considerably among polymer systems and operating conditions. Tab. 2 summarizes the predominant mechanisms for representative polymer tribological systems under different contact and operating conditions. However, quantitative data on the relative contributions of the different dissipation mechanisms remain limited. Existing studies employ different material pairs, operating conditions, spatial-temporal scales, and evaluation parameters, making direct quantitative comparison difficult.

Just Accepted

Tab. 2 Main frictional heat-generation mechanisms in representative polymer systems.

Polymer	Contact and operating conditions	Main mechanism	Reported evidence	Reference
PTFE	Cu/PTFE; planar sliding; 500 MPa; 0.5 Å ps^{-1}; 298.15 K (MD simulation)	Sustained conformational dissipation	Conformational fluctuations persist during 1-10 ns; dissipation is concentrated near the interface with a distinct subsurface temperature peak	[24]
	Fe(001)/PTFE; planar sliding; 100 MPa; 1.47 m/s; 300 K (MD simulation)	Interface-localized non-bonded dissipation	Van der Waals and electrostatic energy dissipation is concentrated near the interface and is accompanied by a pronounced subsurface temperature maximum	[25]
PI	Cu/PI; planar sliding; 500 MPa; 0.5 Å ps^{-1}; 298.15 K (MD simulation)	Limited conformational dissipation associated with high chain rigidity	Conformational rearrangement mainly occurs during 1–4 ns and subsequently stabilizes;	[24]

			the temperature rise is markedly lower than that of PTFE	
POM	Fe(001)/POM; planar sliding; 100 MPa; 1.47 m/s; 300 K (MD simulation)	Distributed conformational dissipation	Bond-angle and dihedral-angle relaxation produces a distributed dissipation zone extending several nanometers into the polymer subsurface	[25]
Rubber	Water/rubber-bearing interface; transient journal-bearing contact under mixed lubrication; dynamic rotor loading and variable rubber relaxation time; water lubrication (Experiment)	Bulk viscoelastic hysteresis and roughness induced viscoelastic dissipation	The viscoelastic contribution to transient friction and total heat flux exceeds the contributions of actual contact shear and fluid shear	[29]
Polyurethane	Polyurethane/cotton-fabric interface; dry sliding against fibrous counterface; variable normal load and sliding speed; ambient conditions (Experiment)	Interfacial shear and plastic dissipation	Irreversible deformation, plastic flow, micro-cutting, and fatigue damage become more significant as contact severity increases; the plastic heat contribution was not separately quantified	[32]
PEEK	PEEK/steel or PEEK/sapphire; ball-on-disc dry sliding; 1 and 40 N at 100 mm/s, or 10 N at 1-4000 mm/s; 25 °C (Experiment)	Interfacial shear and transfer film-controlled heating, with increasing tribochemical contribution under severe conditions	Transfer film formation changes the local contact from PEEK/steel to PEEK/PEEK and substantially alters the predicted flash temperature; individual contributions remain unresolved	[33]

The two PTFE studies listed in Tab. 2 involve different counterfaces and operating conditions. The former study highlights the temporal persistence of conformational fluctuations, while the latter reveals near-interface dissipation dominated by the reorganization of non-bonded interactions. These results indicate that changes in the counterface material, contact pressure, and sliding velocity can modify interfacial interactions and stress transfer behavior, thereby affecting the predominant pathway and characteristics of frictional energy dissipation, even for the same polymer. The mechanisms summarized in Tab. 2 should be regarded as representative pathways under specific conditions rather than universal processes occurring simultaneously in every polymer material. As illustrated in Fig. 3, future studies should focus on quantitatively identifying the relative contribution

Just Accepted

of each mechanism by combining mechanism-specific energy indicators with heat-flux and temperature measurements. To establish the link between microscopic energy conversion and macroscopic temperature rise, Section 3 therefore reviews the methods for calculating and characterizing friction induced temperature.

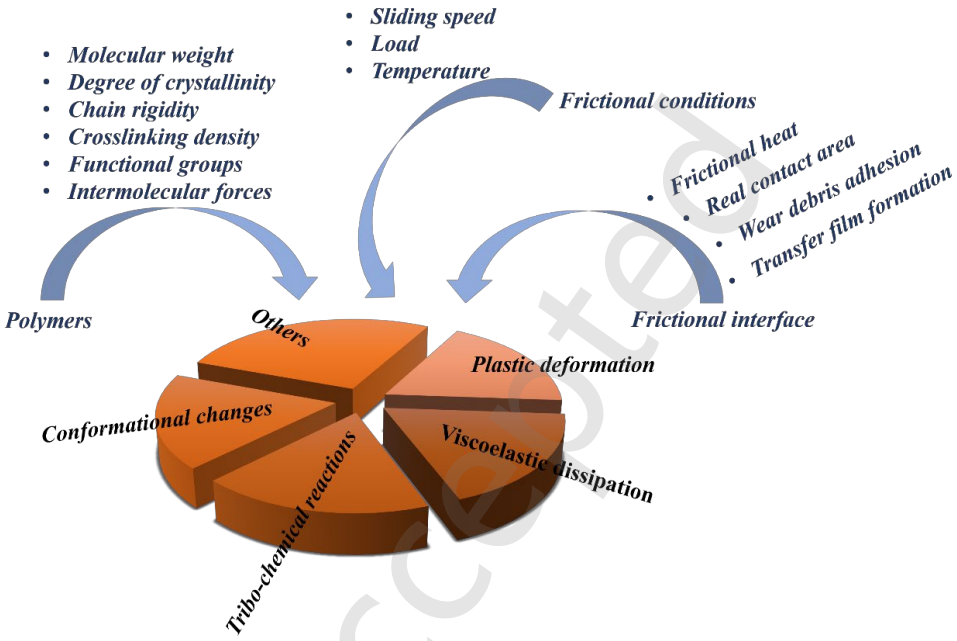


Fig. 3 Schematic diagram of quantitatively identifying the relative contribution of each mechanism under different material systems and friction conditions.

3 Calculation and characterization of frictional heat

Due to the low thermal conductivity and limited thermal diffusivity of polymers [34], they often exhibit more pronounced local temperature rises than metallic systems under the same heat generation conditions. Therefore, accurately calculating the contact temperature of polymer tribo-pairs is essential for understanding their wear mechanisms, predicting service life, and optimizing material design. Research on the temperature rise caused by frictional heat in polymers can be broadly divided into three areas. The first is analytical calculation based on flash temperature theory and moving heat source theory, which mainly reveals the fundamental relationship between frictional work input and the transient interfacial temperature rise. The second is numerical simulation based on the finite element method, which focuses on problems that are difficult for analytical models to

Just Accepted

handle, such as finite dimensions, complex boundaries, material nonlinearity, and the dynamic evolution of heat partition. The third is experimental measurement using techniques such as thermocouples and infrared thermography, aimed at calibrating model results and capturing the temperature response of real friction interfaces.

In 1937, Blok first introduced the concept of flash temperature, noting that actual contact between tribo-pair occurs at asperities. The frictional work is largely dissipated at the real contact points, thereby generating localized instantaneous temperatures far exceeding the average interface temperature [35]. Subsequently, Jaeger developed an analytical model of the sliding contact temperature field based on moving heat source theory. In this model, the frictional contact zone is treated as a moving heat source, revealing the relationship between heat input and thermal diffusion. The Peclet number was introduced to characterize the relative strength between heat advection and thermal diffusion [36]. To facilitate engineering applications, Archard proposed a simplified model for predicting the temperature rise in actual tribo-pairs. This work gradually established flash temperature theory as an important tool for frictional heat analysis [37]. To overcome the limited applicability of conventional models under different sliding speed conditions, Tian and Kennedy employed the Green's function method to develop a flash temperature prediction model that is valid over the entire range of Peclet numbers, thereby improving the accuracy and universality of temperature calculations [38]. The theoretical framework of these classical flash temperature models is general and was not originally developed specifically for polymers. However, driven by the severe thermally induced failures that polymers often suffer in applications, researchers have applied these models to predict temperature rises in polymer-metal tribo-pairs. Based on the flash temperature solution of Tian and Kennedy [38], the steady-state temperature rise solution of Ashby et al. [39], and the steady-state temperature rise solution for disk convection cooling of Laraqi et al. [40], Kennedy et al. [23] developed a temperature prediction method for the pin-on-disk configuration. This method was applied to the design of wear tests for an ultrahigh-molecular-weight polyethylene

Just Accepted

(UHMWPE) pin-on-disk contact, with the aim of determining the safe sliding speed range that avoids thermally induced transitions in wear mechanisms. As research has progressed, the limitations of classical flash temperature models for polymer-metal tribo-pairs have gradually become apparent. First, these models typically treat the contacting bodies as semi-infinite solids, ignoring the effects of sample size and boundary conditions on heat accumulation [23]. They also focus only on the instantaneous temperature rise at the contact interface and do not account for the long-term accumulation of frictional heat within the contacting bodies [21]. Second, polymers tend to form transfer films on the metal counterface during sliding, which alters the actual material pairing at the contact interface. In infrared thermography experiments on PEEK-sapphire and PEEK-steel contacts, Laux et al. [33] found that when the PEEK transfer film formed on the steel counterface, the local contact became a self-mated PEEK-PEEK contact. Since the predicted flash temperature for PEEK-PEEK contact is much higher than that for PEEK-steel contact, the presence of such a transfer film can cause the actual contact temperature to be significantly higher than the value calculated based on the initial material pair. This indicates that the evolution of the friction interface is also a source of deviation in flash temperature predictions.

To overcome the limitations of flash temperature models in handling finite dimensions, complex boundaries, and material nonlinearity, the finite element method (FEM) has been introduced into the calculation of frictional heat for polymer-metal contacts. Mu et al. [41] quantified the influence of material parameters on contact temperature by developing a two-dimensional axisymmetric FEM model of a ring-block contact for PI composites, and systematically analyzed the effects of thermal conductivity and friction coefficient. Their study showed that reducing the friction coefficient by 40% decreased the temperature by approximately 72°C, an effect about 18 times greater than that of an equivalent increase in thermal conductivity. This finding directly indicates that, given the limited scope for improving the thermal conductivity of composites, controlling interfacial friction is more effective in suppressing the heat source itself. Xia et al. [42] developed an FEM

Just Accepted

model that incorporates a time-varying friction coefficient and temperature dependent material parameters. They adopted the total heat flux method, which enforces temperature continuity at the interface to achieve automatic heat flux partitioning. The model revealed that, in polymer-steel friction, the heat partition coefficient is not a constant but evolves dynamically from an initial value to a steady-state value. It is also significantly influenced by geometric parameters such as the polymer contact area and the steel disk thickness. Kalin et al. [21] built a complete three-dimensional FEM model incorporating a steel disk, a PTFE insulating disk, and a polymer pin. The boundary conditions covered three heat transfer mechanisms: convection, conduction, and radiation. Calibrated against an infrared thermography experimental system, the model predicted the temperature field with a relative deviation of 0.4%-2.0% from experimental measurements. Using this model, they obtained the contact interface temperature, which cannot be directly measured experimentally. The results quantitatively revealed that the steady-state temperature rise of the steel disk accounted for 91%-97% of the maximum contact temperature, while the flash temperature contributed only 6%-9%. This demonstrated that, for polymer-metal tribo-pairs, thermal management at the friction interface is more critical than the intrinsic thermal conductivity of the material.

Although the flash temperature models and finite element simulations described above can predict the distribution of the contact temperature field, the accuracy of their results depends on the reasonable specification of input information such as boundary conditions, material parameters, and heat transfer modes. They therefore require calibration and validation through experimental measurements. For this purpose, researchers have developed various methods to measure temperature at or near the friction interface. For contact based thermometry, embedded thermocouples are among the most widely used methods. Mu et al. [41] embedded thermocouples at a distance of 1 mm from the friction interface in ring-on-block tests, and the error between the experimental and FEM-predicted values was kept within 10%. As shown in Fig. 4 (a), Xia et al. [42] implanted thermocouples into the polymer side wall 1.5 mm from the contact surface, with a

Just Accepted

measurement error of 1-2 °C. Kennedy et al. [23] used thermocouples to measure the temperature at the outlet side of the steel disk in PEEK-steel contact, showing that the contact temperature approached the glass transition temperature of PEEK. However, contact thermometry cannot directly capture the interface temperature, and embedded sensors can disturb the local heat flux. For non-contact thermometry, as shown in Fig. 4 (b) and (c), infrared thermography can provide the temperature distribution during the friction process, thereby overcoming the limitation of single-point measurements inherent to thermocouples [32][43]. More recently, luminescence thermometry has been introduced into polymer-gear temperature measurements. It determines temperature from the temperature dependent emission of luminescent particles incorporated into the polymer. This method enables non-contact measurement, but requires optical access and material-specific calibration; moreover, the particles may affect the polymer properties, and the buried contact temperature remains difficult to measure [44].

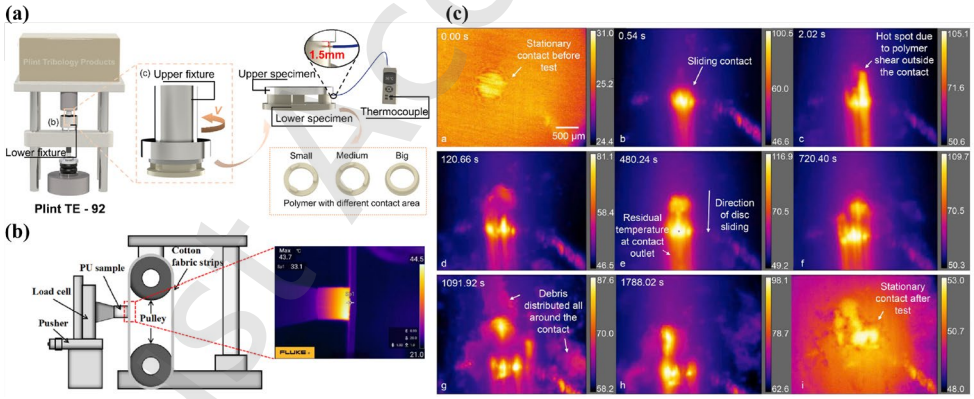


Fig. 4 Representative experimental methods for frictional temperature measurement. (a) Thermocouple based measurement of the temperature near a polymer friction interface [42]; (b) Schematic diagram of the experimental setup and infrared thermography imaging [32]; (c) snapshots of in-situ temperature measurement using IR imaging [43].

Overall, the prediction and characterization of friction induced temperature in polymer tribo-pairs involve complementary analytical, numerical, and experimental approaches. Analytical models provide efficient estimates of local contact temperature but rely on simplified assumptions regarding geometry, material properties, and interface evolution. Finite element models can incorporate finite dimensions, complex boundary conditions, temperature dependent properties, and dynamic heat partition, whereas experimental measurements are required for model calibration and validation.

Just Accepted

Accordingly, these approaches are increasingly used in combination to characterize friction induced temperature in polymer tribological systems. Tab. 3 summarizes the applications, reported errors or uncertainties, spatial and temporal resolutions, limitations, and representative studies of the principal analytical, numerical, and experimental methods. Despite recent progress, existing methods cannot simultaneously resolve localized temperature changes at buried polymer interfaces and identify the mechanical processes responsible for heat generation. Raman thermometry can map local temperature from calibrated spectral changes [54]. Its potential for polymer tribology is supported by Raman temperature measurement in a polymer device [55] and in-operando Raman monitoring of lubricant drainage, wear and internal stress during polymer sliding [56]. Acoustic emission can complement infrared, luminescence or Raman thermometry by detecting transient mechanical events, as demonstrated in PEKK sliding contacts [57]. Combining these methods could link local heating with stick–slip, cracking and debris formation, thereby improving our understanding of how frictional heating affects interfacial behavior and wear evolution.

Tab. 3 Comparison of analytical, numerical and experimental methods for friction induced temperature analysis in polymer tribo-pairs.

Method	Type	Application	Reported error/uncertainty	Spatial resolution	Temporal resolution	Limitations	Reference
Analytical flash-temperature models	Prediction	Estimate mean or maximum contact temperature in pin-on-disc, block-on-ring and gear contacts	-	-	-	Accuracy depends on contact area, heat partition, friction coefficient and temperature dependent properties. Asperity scale flash temperatures are generally unresolved	[21]
Finite-element simulation	Prediction	Calculate transient temperature fields in complex polymer contacts and gears	Experiment-simulation difference: <10% in Mu et al. [41]; experimental thermocouple error: 1-2 °C in Xia et al. [42]	-	-	Strongly dependent on mesh, time step, boundary conditions, thermal contact	[41][42]

Just Accepted

						resistance and temperature dependent material properties Steep temperature gradients cause interface-temperature underestimation. Wires, holes and adhesives may disturb local heat flow	
Embedded/near-contact thermocouple	Indirect measurement	Measure subsurface or bulk temperature in polymer pins, blocks and gears	1-2°C after calibration in Xia et al. [42]	0.1 mm junction scale in Nosko et al. [45]; typical depths: 0.5-1.5 mm from the interface	2 Hz in Nosko et al. [45]		[41][42][45][47]
Grindable thermocouple	Direct, intrusive measurement	Measure sliding-surface temperature in polymers and tyre tread rubber	Average test-retest repeatability: 5.7%; temperature-rise overestimation was 23% compared with the exposed conventional-thermocouple reference	0.34 mm nominal sensing scale, based on tip diameter	2 Hz	The metallic tip participates in friction and may increase local heating. Junction stability decreases at low contact pressure	[45][46]
Point IR pyrometer	Non-contact, single-point measurement	Measure spot-averaged temperature near an exposed polymer contact	-	-	-	No two-dimensional temperature field is obtained. Results depend on spot size, emissivity, roughness and transfer film formation. Buried contacts are inaccessible	[48]
IR thermography	Non-contact, full-field measurement	Map temperature on exposed gear surfaces, tooth flanks and wear tracks	-	-	Approximately 1912 frames s^{-1}; calculated frame interval: 0.523 ms; integration time: 0.1 ms[49]	Closed contacts are obscured. Emissivity varies with polymer type, temperature, roughness, viewing angle and transfer film	[49][50][51]
IR	Non-	Map	-	3 μm for	-	Restricted to	[33][52]

Just Accepted

thermography (through transparent counterface)	contact, full-field measurement	apparent interface temperature through CaF_2 or sapphire		rubber/CaF_2; 6.3 μm for PEEK/sapphire and PBI/sapphire	IR-transparent counterfaces; counterface absorption, reflection and calibration must be corrected; transparent contacts may differ from engineering contacts	[53]
luminescence thermometry	Non-contact optical measurement	Measure friction induced surface heating in polymer gear	Repeatability, expressed as SD of 100 readings: 0.07 K at steady state and 700 rpm. Calibration SD: 0.07-0.10 K over 299-373 K.	-	-	Probe particles may alter mechanical, thermal and tribological properties. Pressure, stress and laser heating effects require validation [44]

Note: Reported performance values are specific to the instrument and experimental configuration. A dash (-) indicates that the corresponding information was not reported.

4 Adverse effects of excessive frictional heat

As frictional heat accumulates at the friction interface, the molecular mobility of polymer chains, interfacial contact characteristics, tribo-chemical reactions, and transfer film evolution continuously change. These thermally induced structural evolutions, in turn, influence friction, wear resistance, and long-term service stability. Because different polymers possess distinct thermal transition temperatures and thermal stability, the same interface temperature may induce different tribological responses in different material systems. Representative thermal references and corresponding tribological responses for different polymer classes are summarized in Tab. 4. It should be noted that the regimes summarized in Tab. 4 are representative rather than fixed temperature boundaries, because the actual thermal response also depends on the contact configuration, load/contact pressure, sliding velocity, counterface material, lubrication or environmental conditions, and heat dissipation characteristics of the tribological system. The glass transition temperature (Tg) provides an important

Just Accepted

thermal reference because the physical state and viscoelastic response of polymers change markedly in its vicinity, often accompanied by pronounced changes in friction and wear [22][66][67]. However, reaching or moderately exceeding Tg does not necessarily imply thermal damage. Enhanced segmental mobility can facilitate interfacial accommodation and stress relaxation, thereby reducing friction and wear in some polymer systems, while thermally activated interfacial processes can also promote the formation of lubricating transfer films [68][69]. Conversely, thermal softening in the glass transition region may destabilize the transfer film and aggravate friction and surface damage under other contact conditions. Therefore, whether frictional heat is beneficial or detrimental depends on the competition between thermally activated interfacial adaptation and heat induced loss of mechanical and interfacial stability. Accordingly, this section focuses specifically on excessive frictional heating, whose adverse effects can be broadly classified into three representative mechanisms: thermal softening of the polymer matrix, chemical degradation, and transfer film failure, as schematically illustrated in Fig. 5.

Tab. 4 Characteristic thermal references of major polymer classes.

Polymer classification	Main thermal reference	Thermal response	Excessive heating response	Representative polymer
Amorphous thermoplastics	Tg	Near Tg, increased segmental mobility strongly alters interfacial shear and may reduce friction/wear in some systems	Further thermal softening reduces mechanical strength and may promote adhesion, cracking, or wear	PVC [58], PMMA [59], PS [60], PC [61],PEI [62]
Semicrystalline thermoplastics	Tg, Tm	Around/above Tg, mobility of the amorphous phase increases while crystallites still constrain flow; transfer layer formation may be promoted	Softening or transfer film instability may develop near/above Tg; toward Tm, crystalline constraint is progressively lost	PAEK [67], PEEK[68]
Thermosets	Tg	Below/near Tg, the crosslinked matrix retains relatively high stiffness and mechanical support	Across/above Tg, glassy to rubbery softening can increase deformation, friction, and wear	Phenolic[63], Polybenzoxazine [64]
Elastomers	Tg/temperature dependent	Typically above Tg, friction is strongly	Large flash-temperature rises	SBR [31], NBR [65]

Just Accepted

	viscoelasticity	governed by temperature dependent deformation and energy dissipation; moderate heating may shift or reduce friction	can strongly alter friction and may induce friction loss or instability

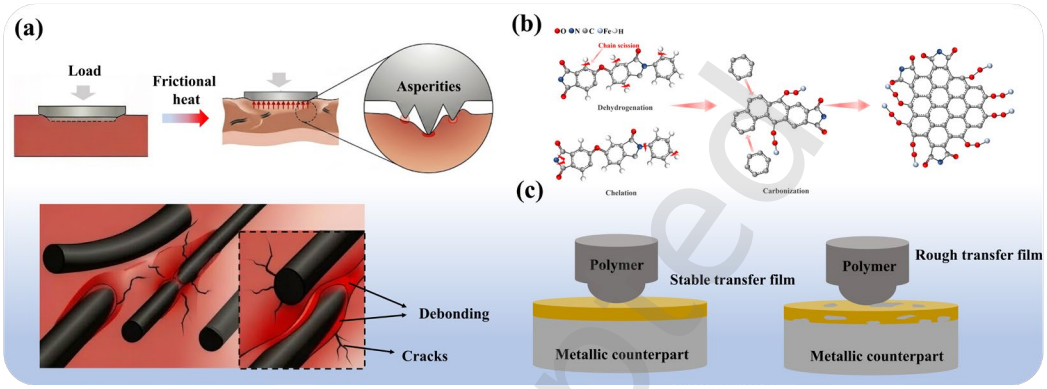


Fig. 5 Adverse effects of frictional heat: (a) thermal softening of the polymer matrix, (b) chemical degradation, (c) transfer film failure.

4.1 Thermal softening of the polymer matrix

Polymers have inherently low thermal conductivity. This restricts the rapid conduction of frictional heat into the bulk material and the external environment, causing substantial heat accumulation near the friction interface. When the interface temperature approaches or exceeds the glass transition temperature or melting point of the polymer matrix, the matrix first undergoes thermal softening. The elastic modulus, hardness, and load-bearing capacity of the matrix then decrease significantly [70]. After thermal softening, the polymer becomes more susceptible to plastic flow and adhesive deformation under the combined action of normal load and tangential shear stress. The softened surface layer continuously undergoes compaction, stretching, and repeated shear, gradually forming an uneven plastic deformation zone. In severe cases, flake-like detachment may occur [11][71]. Meanwhile, the elastic recovery ability of the matrix decreases. This leads to an increase in the real contact area, interfacial shear resistance, and friction coefficient, which further promotes frictional heat accumulation and material wear [72]. When the interface temperature continues to rise and approaches the melting point of the polymer, localized melting flow may even

Just Accepted

occur. This reduces the dimensional stability of the material and severely shortens the service life of the polymer component [33].

Thermal softening weakens the support and confinement provided by the polymer matrix to the reinforcing filler. As the matrix modulus and interfacial bonding strength decrease, load transfer between the matrix and filler becomes inefficient, and stress concentration at the interface intensifies. Under cyclic contact and shear, the filler becomes more prone to debonding, pull-out, or even fracture [73]. Once the filler detaches, the original reinforcing and load-bearing framework of the composite is disrupted. More load then concentrates on the softened matrix, further aggravating local plastic deformation and interfacial stress concentration, and causing a continuous decline in load-bearing capacity. This interfacial bonding failure induced by thermal softening not only undermines the structural stability of the composite, but also adversely affects the stability of the transfer film and the evolution of the friction interface.

4.2 Chemical degradation of the polymer

The rise in interface temperature not only causes matrix softening but also triggers chemical degradation of the polymer chains, such as covalent bond scission, oxidation, or changes in crosslinked structures [74][75]. This degradation is generally irreversible [76].

Main-chain scission is the most typical manifestation of thermochemical degradation in polymers. In phenolic resin-based composites, when frictional heat raises the interface temperature above 350 °C, the resin undergoes thermal cracking and generates a large number of low-molecular-weight gases. These gases accumulate at the friction interface, forming a gas cushion effect. The gas cushion reduces the actual contact pressure and leads to a rapid drop in friction coefficient. This phenomenon is known as thermal fade [77]. In epoxy resin systems, frictional heat induces oxidative scission of molecular bonds in the molecular chains. As a result, the material peels off as debris [78]. Even polyimide, known for excellent heat resistance, remains susceptible to localized thermal degradation under high frictional temperature conditions. Studies show that frictional heat can induce

Just Accepted

selective scission of C-O and C=O bonds in polyimide molecular chains. With the involvement of the metal counterface and lubricant components, further thermochemical reactions occur. As shown in Fig. 6 (a), these reactions generate black degradation products [79]. In addition, localized high temperatures generated by high loads may induce carbonization and ring opening of the imide ring. A schematic of this process is shown in Fig. 6 (b). This further weakens the structural stability of the polymer and aggravates the deterioration of tribological performance [80].

It is worth noting that chemical degradation of polymers is driven by more than frictional heat alone. In studies of PEEK–steel tribo-pairs, the interface temperature was only slightly above the glass transition temperature. The thermal effect alone failed to explain the significant degradation observed. As shown in Fig. 6 (c), subsequent analysis showed that friction plasma generated during sliding and mechanical shear act together. Through free-radical reactions, these factors induce chain scission and crosslinking, which are the primary cause of structural changes in PEEK molecular chains [43].

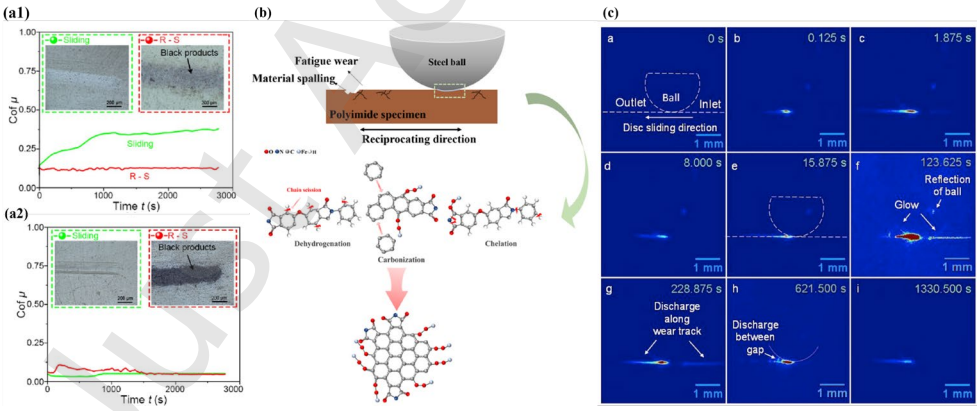


Fig. 6 Representative chemical degradation processes during polymer sliding. (a1, a2) Friction response and wear track evolution of PI under dry and PAO4 lubricated conditions [79]; (b) proposed carbonization and chelation of PI during sliding [80]; (c) optical evidence of friction plasma generated in a PEEK and steel contact [43].

4.3 Failure of the polymer transfer film

The transfer film is critical for reducing interfacial shear resistance and improving friction and wear performance during sliding of polymer composites [81][82]. The continuity, integrity, and stability of the transfer film directly determine the self-lubricating ability of the material. Continuous

Just Accepted

accumulation of frictional heat suppresses the formation of the transfer film. It also weakens the interfacial bonding strength and structural stability of the film, eventually leading to transfer film failure.

The bonding between the transfer film and the metal counterface relies on physical adsorption or chemical bonding. The sustained temperature rise driven by continuous frictional heat causes the film to detach from the counterface surface. The exposed metal surface reveals fresh active sites after detachment. During continuous sliding, adhesion occurs between the metal and the polymer, forming a cycle of adhesion, failure, and readhesion, accompanied by large amounts of wear debris. When the accumulated frictional heat drives the temperature sufficiently high, localized melt welding may even be triggered [83]. After detachment, the transfer film becomes more prone to bulk or flake-like spalling under shear stress. The spalled fragments transform from a lubricating film into abrasive particles, converting two-body wear into more severe three-body wear [84].

Collectively, these degradation modes are strongly coupled rather than independent. The thermomechanical damage described in Section 4.1 increases the supply of detached material and wear debris to the sliding interface. Material transfer is the basis for transfer film development, whereas the size, morphology, adhesion, and persistence of the transferred debris strongly influence whether a continuous and protective film can be established [85][86]. For example, large and loosely adhered debris dominated transfer films can be repeatedly removed during running-in, whereas smaller and more strongly adhered fragments can persist, grow, and merge into a stable transfer film [86]. Therefore, debris generated from a softened and damaged surface may either contribute to transfer film replenishment or, when poorly adhered and continuously removed, disturb the film continuity. Loss of a stable transfer film increases direct interaction between the polymer and counterface and thereby increases interfacial shear and friction. A similar transition has been observed in PAEK mated with steel, where transfer film instability in the glass transition region was accompanied by increased friction and surface damage [67]. The resulting increase in frictional

Just Accepted

dissipation generates additional heat, which can in turn intensify thermomechanical softening and material removal, forming a positive feedback between surface degradation and transfer film instability.

Chemical degradation provides another feedback pathway. As discussed in Section 4.2, tribo-chemical degradation may involve both chain scission and crosslinking. When chain scission predominates, the molecular-weight averages decrease, whereas concurrent crosslinking can partly counteract this change [87]. For polymers exhibiting a Fox-Flory type molecular-weight dependence, a decrease in number-average molecular weight is associated with a decrease in the glass transition temperature [88][89]. Consequently, sufficiently extensive chain scission may shift the near-surface polymer toward a more readily softened state at a given interface temperature, thereby further coupling chemical degradation with thermomechanical softening. This relationship is not universal because the net response depends on the competition among chain scission, crosslinking, oxidation, and other tribo-chemical reactions. For example, as discussed above for PEEK and steel contacts, frictional heating alone is insufficient to account for the observed chemical changes, and mechanically assisted and tribo-plasma related reactions also contribute to the degradation process [43]. Therefore, thermal softening, chemical degradation, and transfer film failure should be regarded as a coupled feedback network whose dominant pathway evolves with the polymer and operating conditions.

Importantly, the accumulation of frictional heat damages both the polymer and the friction interface, and may also cause functional failure or reduced safety of the entire tribological system. In braking systems, heat accumulation causes hot spots and thermal damage. These directly reduce braking safety and service life [90][91]. Under high-speed landing conditions, the tire tread undergoes severe wear and rapid heating due to frictional heat accumulation. In extreme cases, this can even lead to tire blowout [26]. In polymer gear transmission systems, continuous frictional heat raises the tooth surface temperature. This causes a decrease in material hardness and accelerates wear.

Just Accepted

It also leads to increased energy loss, reduced system efficiency, and greater noise and vibration [92]. In artificial joint applications, frictional heat may denature proteins in the synovial fluid. This impairs lubrication and shortens the implant lifespan [93]. Overall, when the interfacial temperature exceeds the thermal tolerance limit of the polymer, the tribological response may shift from mild wear to severe thermal adhesive wear or thermomechanical failure. This ultimately reduces equipment reliability. Although thermal softening, chemical degradation, and transfer film failure are commonly observed, their relative contributions remain highly dependent on the material and operating conditions and have rarely been quantified. Future work should establish quantitative criteria to identify the dominant degradation pathway under different friction conditions.

5 Frictional heat management strategies

To mitigate the adverse effects of frictional heat discussed above, a variety of thermal management strategies have been developed for polymer tribological materials. Thermal management strategies can target different stages of heat generation, transport, accumulation, and interfacial response. According to the primary stage at which they intervene, as shown in Fig. 7, existing strategies can be broadly classified into four categories: (i) enhancing the intrinsic thermal stability of polymers to improve resistance to friction induced thermal damage; (ii) reducing interfacial shear to suppress frictional heat generation; (iii) constructing efficient thermal conduction pathways to accelerate heat transport and dissipation; and (iv) designing surface structures to regulate contact conditions and interfacial evolution.

Just Accepted

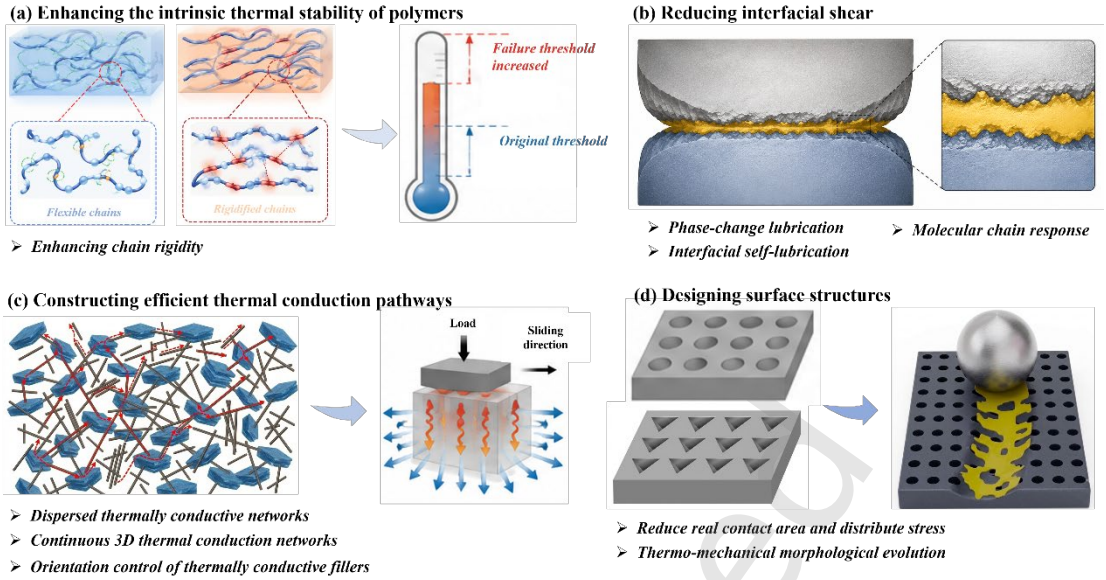


Fig. 7 Schematic diagram of frictional heat management strategies.

5.1 Raising failure threshold via intrinsic thermal stability

Enhancing the intrinsic thermal stability of polymers is a direct strategy for improving their tolerance to frictional heating. As the interface temperature rises during sliding, polymers gradually undergo thermal softening, followed by thermo-oxidative degradation and eventually irreversible structural failure. Therefore, increasing the critical temperature at which these processes occur effectively broadens the operating temperature window and delays friction induced failure.

Molecular-level design of the polymer chemical structure improves the glass transition temperature and intrinsic thermal stability. Fluorine atoms have strong electronegativity and large steric hindrance. Introducing trifluoromethyl groups (-CF_3) into the polymer backbone or side chains significantly increases chain rigidity and the rotational energy barrier, thereby suppressing segmental motion at elevated temperatures. Studies show that incorporating fluorine-containing structures raises the glass transition temperature by approximately 10 °C and simultaneously enhances thermal stability. More importantly, this increased rigidity imparts stronger resistance to thermal softening during friction. Even when frictional heating raises the interface temperature, the molecular chains maintain a relatively stable conformation and load-bearing capacity, leading to a markedly reduced wear rate. Furthermore, the low surface energy of fluorine-containing groups reduces adhesion

Just Accepted

between the polymer and the metal counterface, helping to mitigate adhesive wear at the friction interface[94]. Replacing flexible segments with monomers containing rigid aromatic heterocycles or biphenyl structures significantly reduces the conformational freedom of the polymer backbone and raises the activation energy for segmental motion. This design not only increases the glass transition temperature but also enhances the elastic modulus and shear modulus of the material. Notably, while the increased chain rigidity raises the glass transition temperature and strengthens resistance to thermal softening, it may lead to a higher friction coefficient under dry sliding conditions [95]. Thus, polymer structure should therefore be optimized to balance thermal tolerance and tribological performance.

5.2 Reducing friction to suppress heat generation

5.2.1 Phase-change lubrication

Phase change lubrication uses transient interfacial heating to trigger a phase transition. As the interfacial temperature rises during sliding, the phase-change component undergoes a reversible phase transition, consuming part of the friction-generated heat in the form of latent heat and thereby suppressing further temperature rise. Meanwhile, the phase-transition products generated in situ provide a lubricating medium with low shear resistance, enabling the synergistic regulation of interfacial temperature and lubrication. According to the phase-transition mode, current phase-change lubrication strategies mainly include solid-liquid and liquid–gas phase transitions.

Solid-liquid phase transition can be achieved either through the melting of the polymer itself or through encapsulated phase-change materials. As illustrated in Fig. 8 (a), incorporating polycaprolactone (PCL) into epoxy coatings enables frictional heat to melt the PCL. The resulting liquid polymer, owing to its high viscosity and low shear resistance, spreads over the contact surfaces to form a lubricating film, significantly reducing friction and wear [96]. A similar solid-liquid phase-transition mechanism has also been realized using encapsulated phase-change materials. As shown in Fig. 8 (b), n-docosane encapsulated in MXene-decorated microcapsules was

Just Accepted

incorporated into PPS/PTFE fabric composites. Frictional heat triggers the solid-liquid phase transition of n-docosane, absorbing heat to alleviate thermal accumulation. Simultaneously, the molten alkane is continuously released from ruptured microcapsules and forms a self-lubricating film at the friction interface [97].

In addition to solid-liquid phase transition, liquid–gas phase transition has also been employed for frictional heat regulation by exploiting the high latent heat of water evaporation. As illustrated in Fig. 8 (c), hygroscopic lithium chloride (LiCl) was introduced into porous unsaturated polyester composites. Moisture absorbed from the surrounding environment evaporates once triggered by frictional heat, consuming a considerable amount of friction-generated heat through vaporization. Consequently, the interfacial temperature is effectively reduced, preventing thermal softening of the polymer matrix [98]. Overall, phase-change lubrication converts frictional heat into the driving energy for phase transition, thereby simultaneously dissipating heat and generating lubrication in an adaptive manner. This strategy enables self-responsive thermal management without the need for external energy input. Nevertheless, challenges such as leakage of phase-change materials, limited thermal cycling stability, and insufficient matching between the phase-transition temperature and the actual frictional temperature window still restrict its practical applications [99].

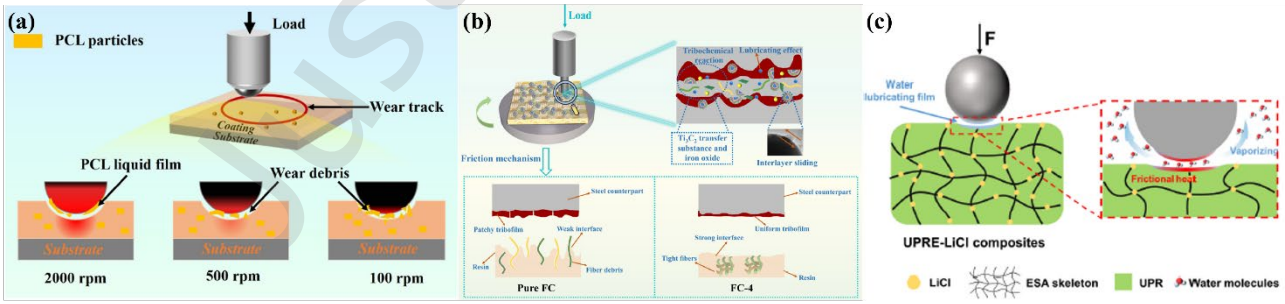


Fig. 8 Representative thermally activated lubrication mechanisms. (a) Solid to liquid transition of PCL and formation of a lubricating film at the sliding interface [96]; (b) friction responsive phase change microcapsules for simultaneous heat absorption and interfacial lubrication [97]; (c) moisture adsorption and evaporation in LiCl containing UPR composites for coupled cooling and lubrication [98].

These limitations may be alleviated by coordinating capsule architecture, phase-transition behavior, and long-term stability rather than optimizing them independently. Strengthening the shell offers an effective way to retain the molten PCM during repeated phase transitions. For instance,

Just Accepted

introducing a secondary SiO_2 layer into paraffin@MF microcapsules decreased leakage by 45.06% while preserving a latent heat above 176 J/g [100], whereas controlled polysiloxane crosslinking of PMMA shells achieved an encapsulation efficiency of 81.3% and a melting enthalpy of 285.0 J/g [101]. Beyond structural stabilization, the phase-transition window itself can be tailored to the expected frictional-temperature range through composition regulation. Paraffin–fatty-acid eutectic systems have demonstrated tunable phase-transition temperatures spanning approximately 49-66°C, providing flexibility for matching PCM activation with different temperature windows [102]. Long-term performance should further be judged by the retention of latent heat and transition temperature, together with leakage and shell integrity over repeated cycles; double-layer ceramic-shell microcapsules, for example, retained more than 90% of their latent heat with almost no leakage after 3000 thermal cycles [103]. Although these strategies have shown promising performance in thermal management, their applicability to polymer tribological materials still needs to be established under the coupled effects of frictional heating, contact pressure, and repeated shear.

5.2.2 Self-lubrication at the sliding interface

Unlike phase-change lubrication, which relies on phase transitions of the material, self-lubrication at the friction interface reduces resistance through the in-situ formation of a low-shear lubricating layer. The main pathways include the formation of a self-lubricating transfer film and the in-situ release of lubricating media. Transfer films generally form through deformation, debris generation, compaction, and interfacial adhesion [75][104]. Under normal load and shear force, frictional heat softens and even locally melts the debris [105][106]. After compaction and spreading, the debris adheres to the counterface [107]. However, films formed by physical compaction have weak bonding and are prone to spalling. In contrast, chemical anchoring driven by moderate frictional heat can firmly bond the film to the metal counterface, thereby enhancing service stability. This mechanism has been confirmed in PEEK [108], PI [109], and PTFE [105]. Fillers can promote transfer film formation through two main mechanisms.

Just Accepted

First, promoting transfer film formation. Layered materials promote transfer film formation through an anisotropic mechanical structure, which combines strong in-plane covalent bonds with weak interlayer van der Waals forces. Under frictional shear stress, relative sliding and exfoliation occur between the layers, forming a low-shear-strength transfer film. This film covers the counterface surface, reduces direct adhesion between the contacting interfaces, and lowers frictional resistance [110][111]. Layered materials such as graphite, hexagonal boron nitride (h-BN), molybdenum disulfide (MoS_2), MXene, and graphene differ in their ability to promote transfer film formation and maintain service effectiveness. These differences arise mainly from the interfacial evolution behavior jointly determined by chemical composition and environmental conditions. For example, the excellent thermal-oxidative stability of h-BN enables the transfer film to remain in a low-shear state under high-temperature conditions [112]. Under high-speed and heavy-load conditions, graphite and the resulting transfer film face a severe risk of oxidative failure. The structural stability declines significantly as the interface temperature rises [113][114]. MoS_2 transfer films are sensitive to high-humidity environments. The edge active sites of the MoS_2 react preferentially with water and oxygen molecules in the air. This generates MoO_3 abrasive particles, which disrupt the layered structure and weaken the lubricating effect [115][116]. MXene is a typical two-dimensional layered material. The intralayer M-X bonds are strong covalent/metallic bonds, while the interlayer bonding relies solely on weak van der Waals forces. Under shear stress, interlayer sliding occurs readily. Abundant surface functional groups, such as -F, -OH, and -O, endow MXene with chemical activity. Under thermo-mechanical coupling conditions, these groups enable MXene to participate in tribo-chemical reactions and form a chemical bonding interface between the transfer film and the counterface [117][118][119]. However, in high-humidity environments, water molecule intercalation expands the interlayer spacing and disrupts the two-dimensional structure, preventing the formation of a dense protective transfer film [120].

Just Accepted

A second approach is to introduce chemically active components that strengthen adhesion between the transfer film and the counterface. For example, Fu et al. [121] found that the addition of Cu nanoparticles significantly promoted the chemical crosslinking reaction between polydopamine (PDA) and the PTFE. This established stronger chemical bonding between PDA and PTFE, thereby improving the interfacial bonding strength of the coating and enhancing the adhesion of the transfer film to the counterpart surface. Similarly, metals such as Ag can generate in situ oxides via tribo-chemical reactions during sliding. These oxides can enhance the mechanical strength of the transfer film and improve its interfacial adhesion [122].

Another approach for interfacial self-lubrication is the in-situ release of lubricating media. This is achieved by incorporating core-shell microcapsules into the matrix to enable friction-responsive release of liquid lubricants [123]. During sliding friction, frictional heat first softens the polymer matrix and reduces the local stress concentration around the microcapsules. This promotes controlled rupture of the shell at a lower contact stress [78]. Subsequently, the rupture of the microcapsule shell releases the encapsulated liquid lubricant to the contact interface. The lubricant spreads rapidly to form a continuous lubricating film [124]. Meanwhile, active groups in the released lubricant, such as Si-OH in silicone oil, undergo dehydration condensation reactions with the polymer matrix under frictional heat. These reactions form Si-O-C covalent bonds and chemically anchor the lubricating film to the counterface. Furthermore, the cavities formed after microcapsule rupture can capture wear debris, reducing damage to the material surface.

5.2.3 Molecular chain response

During friction, polymer molecular chains undergo various structural responses under the action of heat and shear stress. These responses actively regulate frictional heat through mechanisms such as dynamic bond reorganization, structural transformation, and changes in rheological properties.

As shown in Fig. 9 (a), dynamic bond reorganization can reduce interfacial shear through the reversible disruption and reformation of hydrogen bonds. In a polyimide urea copolymer containing

Just Accepted

multiple hydrogen bonds, friction induced temperature rise and shear stress partially disrupt the hydrogen bond network, thereby increasing segmental mobility. The rigid segments subsequently align along the shear direction through π-π stacking, forming a more ordered interfacial structure with lower shear resistance. When the loading conditions change, the hydrogen bonds can reform and the oriented structure can recover. This reversible molecular reorganization helps maintain a low shear interfacial state, thereby reducing the friction coefficient and subsequent frictional heat generation [125].

As shown in Fig. 9 (b), structural transformation achieves surface hardening through friction induced crystallization, reducing the real contact area and interfacial shear resistance, lowering the friction coefficient, and decreasing the conversion of frictional work into heat. Taking polyurea-imide resin as an example, the resin is normally amorphous. During friction, the combined action of interfacial temperature rise and shear stress causes molecular segments to orient along the sliding direction and fold into ordered crystals, a process known as friction induced crystallization. The formation of crystalline regions increases the hardness and shear resistance of the friction surface. Meanwhile, this entropy decreasing process directly consumes part of the frictional heat, helping to prevent thermal softening of the polymer [126].

As shown in Fig. 9 (c), as the temperature approaches or exceeds Tg, increased segmental mobility alters the rheological response of the surface layer. The segments then align along the sliding direction, reducing the friction coefficient and suppressing frictional heat accumulation at the source. Polyvinyl chloride (PVC) has a glass transition temperature of approximately 30 °C. Below Tg, segmental mobility is restricted. The segments cannot relieve shear stress through conformational adjustments, so the friction coefficient remains high and considerable frictional heat is generated. When the interfacial temperature rise exceeds Tg, segmental mobility increases and the segments align along the sliding direction. Through conformational adjustments, the segments adapt to the counterface micro-topography, relieving stress concentration and frictional resistance and

Just Accepted

significantly lowering the friction coefficient. Meanwhile, the softened wear debris curls and rolls between the interfaces, converting part of the sliding friction into rolling friction and further reducing the friction coefficient. The reduction in friction coefficient directly decreases the input of frictional work, thereby suppressing the continuous accumulation of frictional heat at the source [58]. More generally, the temperature frequency dependence discussed in Section 2 can be used to identify operating regions associated with high viscoelastic loss. For material design, polymers with suitable Tg and relaxation characteristics can be selected so that the expected contact temperature and deformation frequency remain away from these high loss regions. For operating conditions, sliding velocity, surface roughness, and heat dissipation can be regulated to further limit viscoelastic energy loss and the associated frictional heat generation.

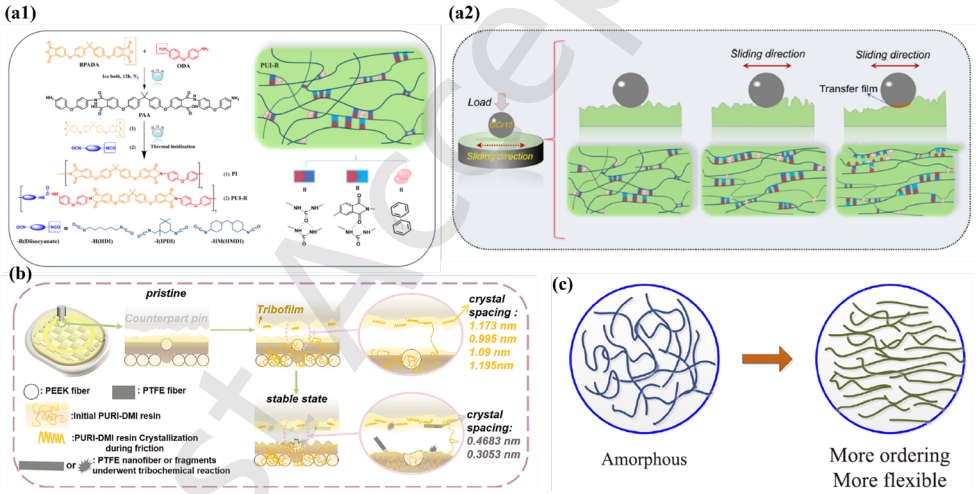


Fig. 9 Molecular chain responses that reduce frictional heat generation. (a) Dynamic bond reorganization and transfer film formation in PUI-H [125]; (b) friction induced crystallization and interfacial evolution in PURI-DMI [126]; (c) increased segmental ordering associated with temperature activated molecular mobility [58].

The friction source suppression strategies discussed above operate through different activation mechanisms and therefore exhibit distinct applicable conditions. Phase change lubrication relies on a defined thermal trigger, conventional self-lubrication provides persistent or replenishable low shear interfaces, whereas molecular chain responses require suitable bond dynamics, crystallizability, or segmental mobility. Tab. 5 compares representative quantitative improvements together with the operating conditions for which each strategy is most appropriate and its principal limitations. These

Just Accepted

strategies primarily regulate frictional heat by reducing interfacial shear or by exploiting frictional heat to activate adaptive lubrication. When heat generation cannot be sufficiently suppressed, accelerating heat removal from the contact becomes a complementary requirement, motivating the thermally conductive network strategies discussed in Section 5.3.

Tab. 5 Quantitative comparison, applications and limitations of strategies for reducing friction to suppress heat generation. (COF means coefficient of friction)

Strategy	Representative sample	Key quantitative value	Best suited conditions and applications	Limitations	Reference
Solid liquid phase change lubrication	10 wt% PCL/EP	COF: ↓50.6%; wear rate: ↓93.1%	Contacts experiencing repeated temperature excursions into a designed phase transition range, where simultaneous friction reduction and temporary heat absorption are required	Performance is strongly dependent on reaching the transition temperature; long term phase cycling and structural stability require consideration	[96]
Liquid gas phase change lubrication	2 wt% LiCl/UPR	Wear rate: ↓88.7%; contact temperature: ↓62.0%	Contacts operating in moisture accessible environments where adsorbed water can provide lubrication and evaporation can remove frictional heat	Strong dependence on environmental humidity and water replenishment; effectiveness decreases when moisture supply is insufficient	[98]
Transfer film self-lubrication	PDA/Cu modified PTFE	Wear rate: ↓53.5%	Dry sliding contacts requiring sustained self-lubrication through the formation of a stable, low shear transfer film on the counterface	Performance depends on transfer film formation, adhesion, and stability; weak interfacial bonding, oxidation, or environmental sensitivity can cause film disruption	[121]
Friction induced lubricant release	15 wt% PMPS@PI/PEEK–PTFE	COF: ↓68.82%; wear rate: ↓98.53%	Dry sliding systems under variable loads and temperatures where on demand lubricant release helps maintain a stable low friction interface	Lubricant supply is finite; capsule integrity and rupture timing directly affect durability and repeatability	[124]
Dynamic bond reorganization	PUI-H	COF: ↓72.4%; wear rate: ↓85.2%	Adaptive polymer interfaces in which shear and moderate frictional heating can activate reversible intermolecular bond rearrangement while retaining structural	Highly dependent on molecular chemistry; long term reversibility and cycling stability under different temperatures and	[125]

Just Accepted

			support	environments require further validation	
Friction induced crystallization	PURI-DMI	COF: ↓ ≈4%; wear rate: ↓ ≈26% (when rotational speed increased from 360 to 800 r/ min)	Crystallizable polymer matrices subjected to sustained shear and frictional heating that can promote local chain ordering without entering the thermal damage regime	Requires sufficient chain mobility and crystallizability; response depends strongly on temperature, shear history and initial molecular structure	[126]
Tg mediated segmental mobility	PVC	COF: ↓≈13%; wear rate: ↓≈11% (when temperature increased from 20 to 50℃)	Amorphous polymers operating near a controlled glass transition window, where moderate heating can activate segmental mobility and interfacial stress relaxation	Beneficial temperature range is limited; excessive heating can cause excessive softening and loss of mechanical support	[58]

Note: Relative change in the reported property compared with the control/reference sample defined in the original study under the same test conditions

5.3 Building thermally conductive networks to accelerate heat dissipation

5.3.1 Dispersed thermally conductive network

The effectiveness of dispersed thermally conductive networks depends strongly on filler size, dimensionality, and connectivity. Micron sized fillers often require relatively high loadings to establish continuous heat transport pathways, whereas nanofillers are more susceptible to agglomeration and interfacial thermal resistance. Combining fillers of different scales and dimensionalities can exploit their complementary structural functions and improve both network continuity and interfacial stability [90][127].

In multiscale thermally conductive networks, zero-dimensional fillers can act as thermally conductive nodes that shorten local heat transport distances and also contribute to load support during sliding. However, isolated particles cannot independently establish long range heat transport pathways. One-dimensional fillers can bridge separated conductive units and construct extended thermal transport frameworks, while also improving deformation resistance and suppressing filler debonding. Two-dimensional fillers provide large contact areas and high in plane thermal conductivity, facilitating heat spreading through lamellar contacts. Their combination therefore

Just Accepted

improves connectivity among conductive units, shortens heat transport distances, and enhances the continuity and stability of the thermal network.

Representative multiscale architectures are shown in Fig. 10. As shown in Fig. 10 (a), the combination of one dimensional and two-dimensional fillers forms a line plane conductive network with numerous contacts among the fillers, thereby reducing interfacial thermal resistance [128]. In Fig. 10 (b), metal and diamond particles are codeposited on carbon fibers to construct a rod on particle thermal transport structure. The carbon fibers provide the conductive framework, whereas the diamond particles act as high thermal conductivity nodes, together forming three-dimensional heat transport pathways [129]. These multiscale architectures can promote frictional heat dissipation while also contributing to load support and interfacial stability.

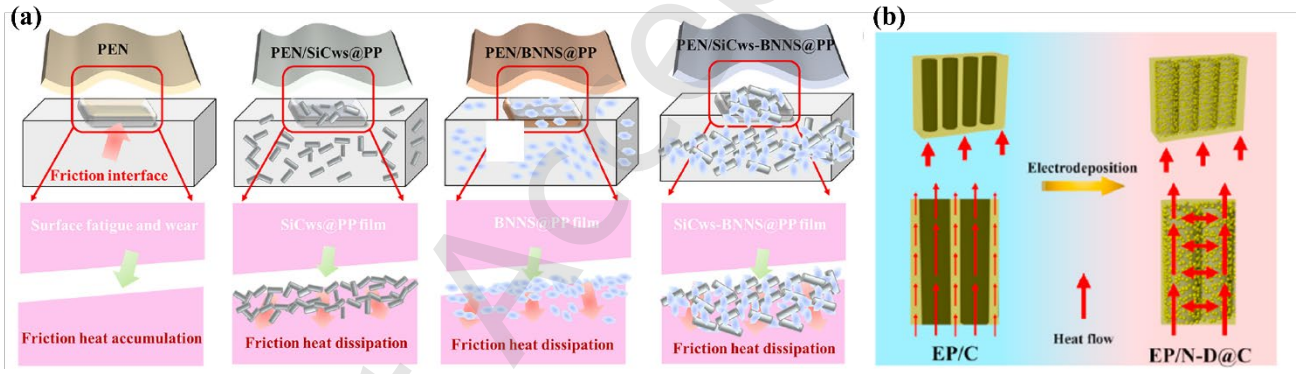


Fig. 10. Heat transfer mechanisms in dispersed thermally conductive networks. (a) Frictional heat dissipation through multiscale conductive fillers in PEN composites [128]; (b) representative thermal conduction pathway formed by a carbon fiber based hybrid conductive network [129].

5.3.2 Continuous 3D thermal conduction network

In a polymer matrix, conventional randomly dispersed thermally conductive fillers are limited by the interfacial thermal resistance between the matrix and the fillers and by the discontinuous contact among the fillers. A high filler loading is usually required to form effective thermal conduction pathways. However, high filler loading often causes the deterioration of mechanical and tribological properties [130]. To address this, constructing a continuous three-dimensional thermally conductive network inside the matrix can achieve enhanced thermal conductivity at lower filler loadings.

Just Accepted

As shown in Fig. 11, three-dimensional open-cell metal foams, such as copper and nickel, rely on a heat conduction mechanism dominated by free electrons. The interconnected pore-wall structure forms a three-dimensional heat transport backbone within the polymer matrix. When frictional heat is generated at the contact points, free electrons in the metal skeleton rapidly transport heat from the high-temperature zone to the low-temperature zone, avoiding the formation of localized hot spots [18][84]. The key structural parameter of this strategy is the pore density of the metal skeleton, expressed as PPI (Pores Per Inch). A higher PPI means a denser distribution of the metal skeleton per unit volume, and the number of available channels for heat conduction along the metal network increases. At the same time, the finer skeleton structure enlarges the interfacial contact area between the metal and the polymer matrix. This facilitates heat transfer from the low thermal conductivity polymer matrix to the high thermal conductivity metal network, reducing the interfacial thermal resistance. The two factors work synergistically, so the effective thermal conductivity is positively correlated with the pore density [131]. Meanwhile, the normal stiffness of the continuous metal network provides mechanical support to the polymer and restricts plastic deformation of the matrix under load. However, mismatch in the coefficients of thermal expansion of the metal and polymer inevitably generates micron-scale interfacial gaps during high-temperature curing or frictional temperature rise. These interfacial gaps partially reduce the interfacial heat conduction efficiency [18][84].

Just Accepted

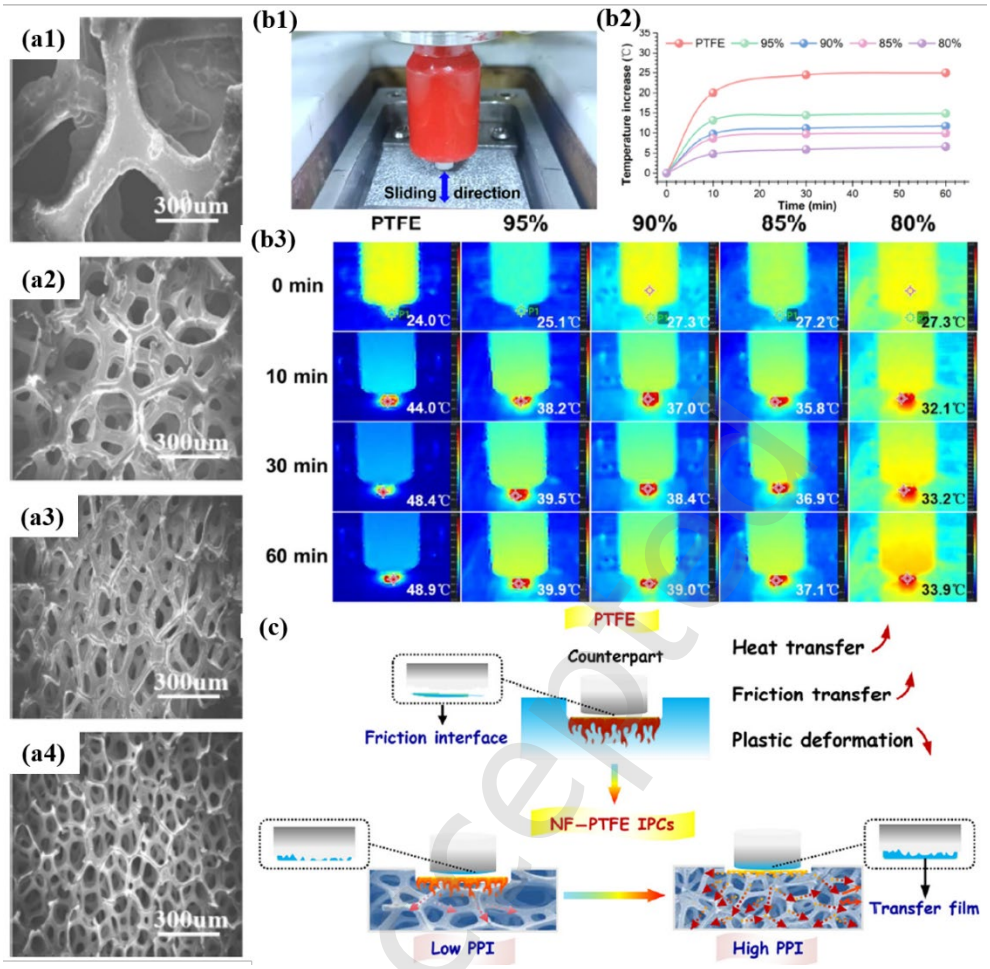


Fig. 11 Representative continuous 3D thermal conduction networks and their heat transfer behavior. (a) Representative Cu foam structures with different pore densities [131]; (b) interfacial temperature response and infrared thermal distribution during sliding in a metal network reinforced polymer composite [18]; (c) proposed friction, wear, and heat transfer mechanism of NF-PTFE interpenetrating composites [84].

Gelation strategies use chemical crosslinking or strong hydrogen bonding to enable dispersed two-dimensional nanosheets and one-dimensional nanofibers to spontaneously assemble into a three-dimensional hydrogel framework in solution. Freeze-drying then yields a continuous porous network structure [12][132]. The network forms through hydrogen bonding between nano-units and reactions between crosslinking agents and functional groups on the filler surfaces. The hydrogen bonding and crosslinking reactions connect the individually dispersed nano-units into an integral whole [133]. In the three-dimensional network, fillers form continuous thermal conduction pathways through covalent bonds or physical contacts, reducing the interfacial thermal resistance caused by discontinuous filler contacts in conventional randomly dispersed systems [134]. When the composite system is subjected to frictional loads, the thermally conductive network rapidly conducts heat away

Just Accepted

from the friction interface. The rapid heat conduction suppresses the formation of local hot spots and slows the thermal softening and thermal degradation of the resin matrix [12][132]. The gelation based network offers a highly tunable network architecture; the pore size and orientation can be controlled by adjusting the filler concentration and freezing conditions [12]. However, volume shrinkage during drying and the insufficient stability of the carbon-based skeleton in high-temperature oxidative environments remain concerns for practical applications.

5.3.3 Orientation control of thermally conductive fillers

Besides enhancing the continuity of thermally conductive networks, the spatial arrangement of thermally conductive fillers also determines the transport path of frictional heat. Since frictional heat is primarily generated at the material surface, heat can either spread along the friction surface to the surroundings or be conducted along the thickness direction into the material interior. Therefore, aligning thermally conductive fillers through external fields can not only enhance thermal conduction efficiency but also enable directional control of heat flow.

As shown in Fig. 12(a), when the filler orientation is parallel to the friction surface, adjacent fillers interconnect along the in-plane direction, forming continuous thermal transport pathways. These pathways enable heat to spread rapidly along the surface and effectively reduce the temperature of localized hot spots. If the filler alignment direction is also parallel to the sliding direction, the lamellar structure can maintain an ordered arrangement and form a continuous and stable low-shear interface. The frictional stress then remains at a low level [71][135].

Fig. 12 (b) shows the effect of graphene orientation on tribological properties of organic coatings. When the fillers are oriented perpendicular to the friction surface, they form directional thermal conduction channels through the thickness. As the orientation angle increases, the heat dissipation rate of the coating in the thickness direction rises. Frictional heat is then rapidly transferred into the material interior or toward the opposite heat sink, reducing heat accumulation at the surface. Meanwhile, the normal elastic modulus reaches the highest value under vertical

Just Accepted

orientation. This enhances the normal load-bearing capacity and helps maintain the stability of the friction interface [136].

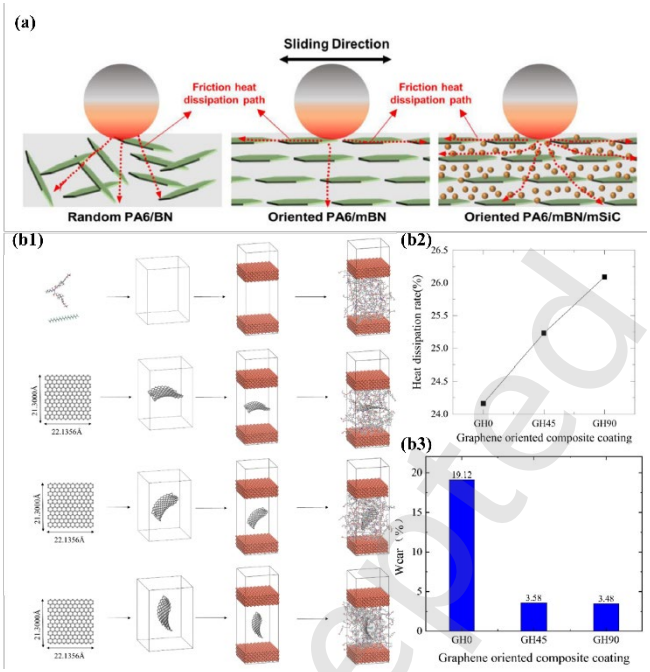


Fig. 12 Effect of filler orientation on frictional heat transport and tribological performance. (a) Heat transfer routes in random and oriented PA6 based thermally conductive networks [71]; (b) representative graphene orientation model and corresponding changes in heat dissipation rate and wear scar [136].

The network architectures described above differ not only in heat transport efficiency but also in filler organization, directional dependence, processing route, and compatibility with different component geometries. Tab. 6 compares representative dispersed, continuous 3D, and oriented networks in terms of thermal and tribological improvements, suitable application conditions, and practical limitations. Despite the considerable improvement in thermal conductivity, the overall heat transport efficiency of polymer composites is not determined solely by the architecture of the conductive pathways. Heat transfer across the numerous polymer-filler and filler-filler interfaces is frequently impeded by interfacial thermal resistance, which has become one of the major factors limiting further enhancement of thermal conductivity. Therefore, quantitative evaluation of interfacial thermal resistance (ITR) is essential for understanding heat transport mechanisms and guiding the rational design of thermally conductive networks. Representative analytical, empirical, and simulation approaches that have been developed for this purpose are summarized in Tab. 7. These models provide valuable theoretical guidance for interface modification and thermal network

Just Accepted

optimization, although accurately describing the dynamically evolving interfaces under frictional conditions remains challenging.

Tab. 6 Quantitative comparison and applicability of representative thermally conductive network strategies. (TC means thermal conductivity, COF means coefficient of friction)

Strategy	Representative sample	Key quantitative value	Best suited conditions and applications	Limitations	Reference
Dispersed thermally conductive network Multidimensional dispersed network	h-BN filled brake friction composite	TC: ↑62.8%	Polymer friction composites where thermally conductive fillers can be directly incorporated into the matrix to improve heat dissipation while retaining the original composite architecture	Effective heat transport depends on filler dispersion and contact between conductive units; relatively high filler contents may be required to establish continuous heat transfer pathways	[90]
	PEN/SiCws–BNNS@PDA–PEI	TC: ↑189.11%; COF: ↓45.16%; wear rate: ↓87.57%	Same as above	Same as above	[128]
	PPS@PDA–CNTs–SiC	TC: ↑120%; COF: ↓18.9%; wear rate; ↓50.0%	Same as above	Same as above	[73]
Continuous 3D thermal conduction network	0.75 wt% C CNT/130 PPI Cu foam/EP	TC: ↑54.8%; COF: ↓9.5%; wear rate: ↓40.6%	Polymer composites where a continuous conductive skeleton can be incorporated into the matrix to provide persistent heat transfer pathways and mechanical support	Thermal expansion mismatch between metal and polymer can generate interfacial gaps and reduce heat transfer efficiency; the matrix must also adequately infiltrate the porous skeleton	[131]
	RGO/Si_3N_4 hybrid aerogel/EP	TC: ↑45.4%; COF: ↓83.7%; wear rate: ↓35.8%	Resin based tribological composites where a preformed porous network can provide continuous heat transfer pathways and	The preparation process is complex, drying shrinkage and the oxidative stability of skeletons remain practical concerns	[134]

Just Accepted

			suppress local frictional heat accumulation		
Oriented network Oriented hybrid network	SiC packed BN/PA6	In plane TC: ↑352%; through plane: TC: ↑25%; wear rate: ↓92.5%	Filler alignment can be designed to spread frictional heat along the required direction	Thermal enhancement is strongly direction dependent; the benefit decreases when filler orientation does not coincide with the required heat transfer direction	[71]

Note: Relative change in the reported property compared with the control/reference sample defined in the original study under the same test conditions

Tab. 7 Representative methods for analyzing interfacial thermal resistance in polymer thermal conduction networks (R denotes the interfacial thermal resistance).

Method	Filler geometry	Key formula/approach	Reference
EMA (Maxwell-Garnett)	Spherical, ellipsoidal	$\frac{K_e}{K_m}=1+\frac{fp}{3}\frac{\frac{K_c}{K_m}}{p+\frac{2RK_m}{d}\frac{K_c}{K_m}}$	[137]
EMA (with h_c)	Spheres, circular cylinders, flat plates	$K_{eff}=Km\frac{2\left(\frac{K_d}{K_m}\frac{K_d}{ah_c}-1\right)V_d+\frac{K_d}{K_m}+\frac{2K_d}{ah_c}+2}{\left(1-\frac{K_d}{K_m}+\frac{K_d}{ah_c}\right)V_d+\frac{K_d}{K_m}+\frac{2K_d}{ah_c}+2}$, $R=\frac{1}{h_c}$	[138]
NEMD	Graphene/graphite (2D sheets)	$R=\frac{\Delta T}{J}$	[139]
Foygel theory	2D sheets	$R=\frac{1}{k_0\times L\times(\phi_c)^{\tau}}\frac{2d^2}{\Pi}ln[\frac{\sqrt{1+p^{-1}}+1\sqrt{1-p^{-1}}}{\sqrt{1+p^{-1}}-\sqrt{1-p^{-1}}}]$	[128]
Percolation theory	2D sheets	$K_x^c=\frac{K_p}{\frac{2RK_p}{L}+1}$	[140]

Representative applications further demonstrate how these models can quantitatively guide network optimization. For EMA models, Macedo and Ferreira incorporated ITR into the prediction of polymer/carbon-fiber composites and extracted thermal contact resistance from experimentally measured thermal conductivity. The calculated values agreed well with theoretical predictions,

Just Accepted

showing that effective-medium models can quantitatively evaluate the coupled effects of filler size, volume fraction, and interface resistance and can estimate the attainable thermal conductivity of a composite [141]. For molecular dynamics based interfacial analysis, Shen et al. combined molecular dynamics simulations with experiments for graphene/epoxy composites. The simulations showed that both graphene thermal conductivity and heat transfer across the graphene-epoxy interface increased with graphene layer number, while experiments confirmed that graphite nanoplatelets with >10 layers and lateral dimensions >30 μm achieved approximately 1.5 W/(m·K) at only 2.8 vol%, demonstrating that filler thickness and lateral size must be optimized simultaneously to reduce interfacial transport losses while maintaining a high aspect ratio [142]. For percolation modeling, Sarikhani et al. developed a generalized framework and experimentally validated it using a three-dimensional segregated MWCNT/polypropylene network. The model identified a thermal percolation threshold of approximately 1.5 vol% and was further validated against 23 independent datasets containing more than 350 experimental and numerical data points, demonstrating its utility for determining the minimum filler loading required to establish continuous heat-conduction pathways [143]. Together, these cases show that effective medium models quantify the penalty imposed by interfacial resistance, molecular simulations identify the nanoscale structural parameters controlling interfacial heat transfer, and percolation models determine the critical filler content for network formation. Nevertheless, direct quantitative validation of these models under dynamically evolving sliding interfaces remains limited.

5.4 Regulating interfacial contact and morphological evolution

In addition to building thermal conduction pathways inside the material to promote heat dissipation, surface micro/nano structures can also be designed. These structures use geometric modification to regulate the contact state, stress distribution, and thermal conduction path at the friction interface, thereby suppressing frictional heat generation and accelerating heat dissipation. As shown in Fig. 13, surface textures on composites can turn the originally continuous friction interface

Just Accepted

into discrete point or line contacts. This significantly reduces the real contact area. Concentrated loads are then distributed among multiple local contact points, preventing the formation of a single high-pressure zone. As a result, plastic deformation accumulation and instantaneous high temperatures caused by stress concentration are suppressed [144][145]. Notably, in the above studies, circular dimples and pentagonal surface textures exhibited better performance. In contrast, shapes with sharp corners or right angles, such as triangles and grid intersections, caused localized stress concentration and increased deformation. Therefore, surface texture design should prioritize geometries with gentle curvature and rounded corners to minimize stress concentration and thermal and mechanical damage. On the other hand, under dry friction conditions, wear debris acts as third-body abrasive particles, rolling or sliding at the interface and causing additional plowing and micro-cutting. This process aggravates material loss and produces additional heat through frictional dissipation associated with debris motion. The dimples or grooves of surface textures can trap wear debris, thereby reducing the extra heat generated by debris movement.

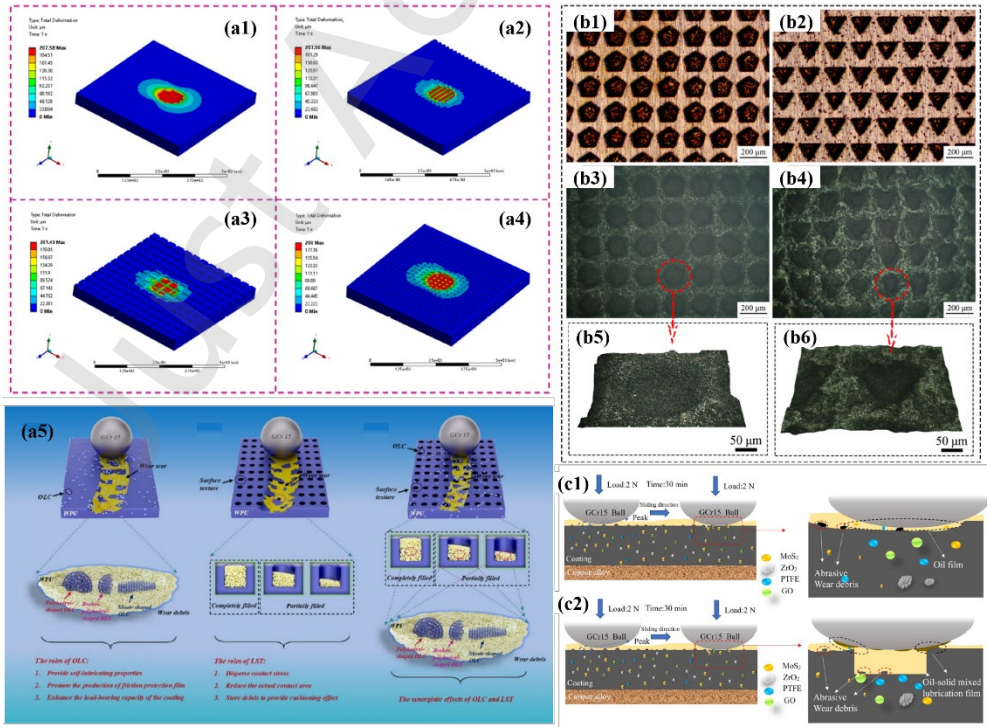
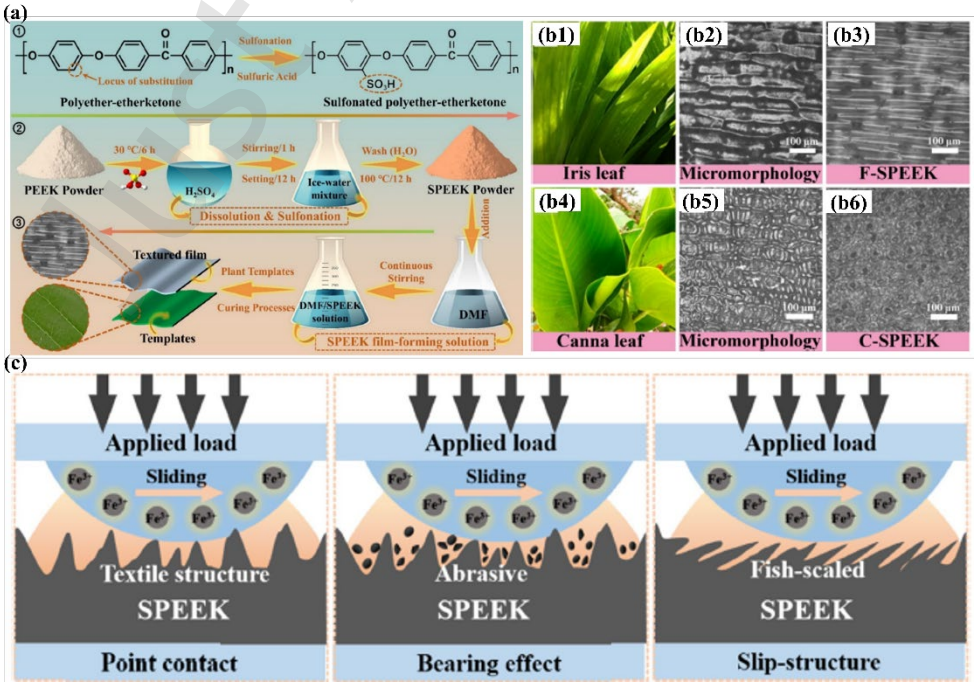


Fig. 13. Effects of surface texturing on contact deformation and interfacial friction. (a1-a4) Total deformation distributions of the untextured surface and three representative textured surfaces, and (a5) proposed mechanism of friction reduction and wear suppression [144]; (b1-b6) representative morphologies of different microtextured surfaces; (c1, c2) schematic comparison of the frictional contact on smooth and pentagonal textured surfaces [145].

Just Accepted

Besides altering the contact state and storing wear debris, surface textures undergo plastic deformation and morphological evolution under frictional heat and shear stress. Because of the low thermal conductivity of polymers, stress concentration at micro-asperities promotes local heat accumulation and thermal softening. Under the combined action of normal load and tangential force, as shown in Fig. 14, the softened asperities undergo plastic deformation and tilt along the sliding direction, gradually transforming from the original square shape into a fish-scale-like morphology. The fish-scale-like surface has reduced roughness. The layered morphology facilitates interlayer sliding under shear. The interlayer sliding reduces interfacial stress transfer. During prolonged friction, the fish-scale-like layer continuously undergoes mild wear and re-forms. Frictional heat maintains the surface softening, allowing the deformed layer to self-regulate and sustain a low-friction state. Note that the sulfonated polyetheretherketone (SPEEK) used in the study possesses high thermal stability and did not undergo chemical degradation within the friction induced temperature rise range investigated [146][147]. However, for other polymers with lower thermal stability, the possibility of concurrent chemical changes should therefore be evaluated for each polymer system.



Just Accepted

Fig. 14 Biomimetic surface textures and friction induced morphological evolution of SPEEK films. (a) Schematic preparation of SPEEK self-lubricating films; (b1–b3) iris inspired texture, including the natural surface, its characteristic morphology, and the corresponding textured SPEEK film; (b4–b6) canna inspired texture and the corresponding surface morphology of the textured film; (c) proposed evolution of the textured surface and its self-lubricating mechanism during sliding[146].

Overall, these frictional heat management strategies involve distinct trade-offs and should not be directly ranked because the reported polymer systems, contact configurations, loads, sliding velocities, temperatures, environments, and test durations differ considerably among studies. Intrinsic thermal stabilization improves resistance to thermal softening but may restrict segmental mobility, whereas friction reduction strategies depend on the stability or activation of lubricating mechanisms. Thermally conductive networks facilitate heat dissipation but may require increased filler loading or additional network fabrication, while oriented structures are strongly dependent on the match between filler orientation and heat flow direction. Therefore, strategy selection should consider the dominant thermal bottleneck together with load, sliding speed, operating temperature, polymer thermal stability, friction and wear requirements, processability, manufacturability, and cost. Under severe conditions, suppressing heat generation and accelerating heat dissipation may need to be considered together rather than optimized independently. Accordingly, the selection of an appropriate thermal management strategy should be based on the dominant issue under the target operating conditions. As summarized in Fig. 15, the different regulation strategies can be selected according to the major thermal bottleneck while simultaneously considering practical constraints such as processability, durability, and manufacturability.

Just Accepted

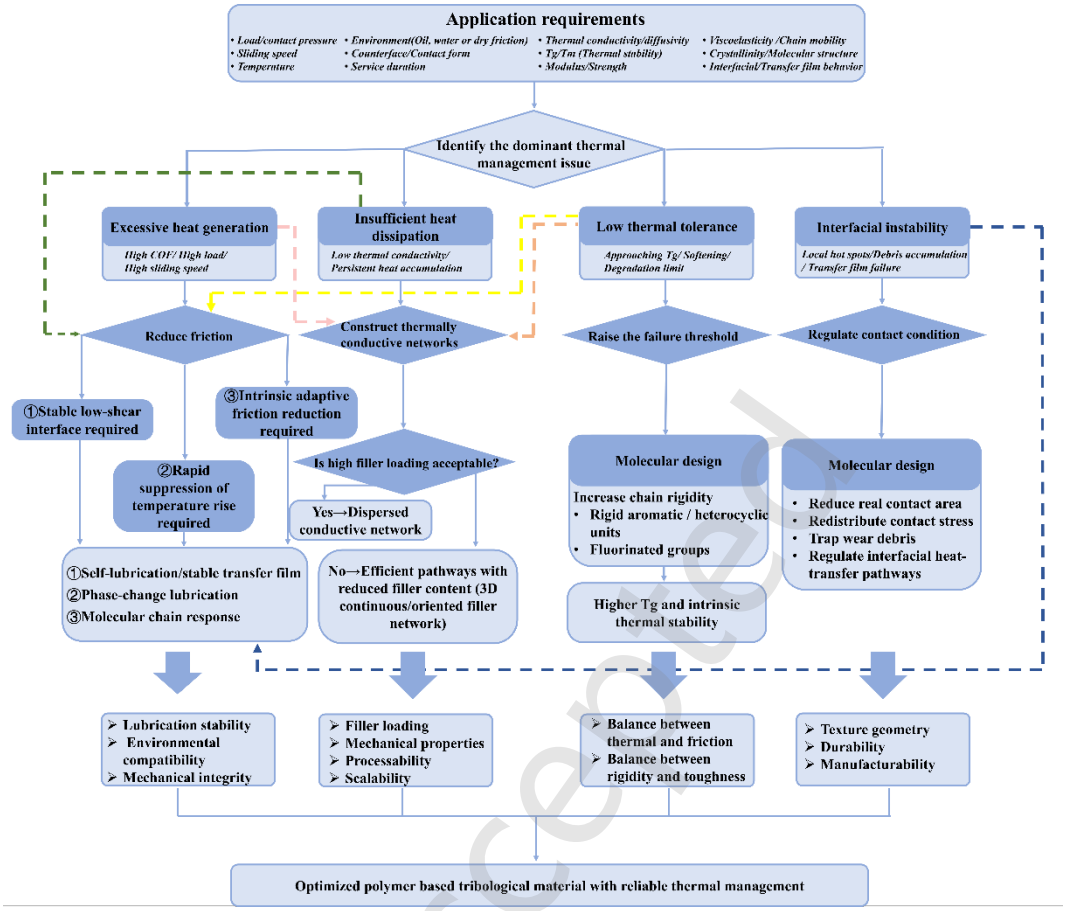


Fig. 15 Decision flowchart for selecting frictional heat management strategies in polymer tribological materials.

6 Conclusions and prospects

During sliding, frictional heat is continuously generated, accumulated, and dissipated while interacting with molecular chain motion, interfacial contact evolution, tribo-chemical reactions, and transfer film formation. These coupled thermo-mechanical processes determine the evolution of the friction interface and ultimately control the friction coefficient, wear resistance, and long-term service reliability of polymer composites. Therefore, understanding frictional heat requires moving beyond temperature rise alone and establishing the intrinsic relationship between frictional heat evolution and interface structural evolution. Existing studies have demonstrated that frictional heat originates from the combined contributions of multiple mechanisms, including molecular chain conformational changes, viscoelastic dissipation, interfacial shear, localized plastic deformation, and tribo-chemical reactions. The development of flash temperature models, finite element simulations,

Just Accepted

and experimental characterization techniques has significantly improved the understanding of friction induced thermal behavior. Meanwhile, frictional heat exhibits a distinct dual effect. When the interface temperature remains within the thermal tolerance window of the polymer, appropriate frictional heating can promote molecular chain mobility and transfer film evolution, thereby improving tribological performance. However, excessive heat accumulation gradually drives the friction interface into the thermal damage regime, resulting in matrix softening, chemical degradation, transfer film failure, and ultimately accelerated wear and premature material failure. To regulate frictional heat, considerable efforts have been devoted to improving the intrinsic thermal stability of polymers, suppressing frictional heat generation, accelerating heat dissipation, and optimizing interfacial contact conditions. Although these strategies intervene at different stages of frictional heat evolution, they share the common objective of regulating heat generation, heat accumulation, and thermal damage throughout the friction process. Future thermal management should therefore shift from optimizing individual material properties toward coordinated regulation of the entire thermal evolution process.

Despite substantial progress, important gaps remain in mechanistic understanding and engineering translation. The main problems in current research are as follows:

(1) Quantitative identification of frictional heat generation mechanisms remains insufficient. Frictional heat originates from the coupling of multiple mechanisms. However, the relative contribution of each heat source under different material systems and operating conditions remains unclear, and systematic quantitative methods capable of separating these contributions are still lacking. This limitation hinders mechanism oriented thermal management and material design.

(2) Reliable criteria for distinguishing beneficial and detrimental frictional heat have not yet been established. Existing studies frequently evaluate thermal effects using characteristic temperatures such as the glass transition temperature or melting temperature. Nevertheless, the thermal response of polymer tribological systems is governed by the combined effects of material

Just Accepted

thermal tolerance, heat accumulation, loading conditions, sliding parameters, counterface characteristics, environmental media, and interface evolution. Establishing reliable criteria capable of quantitatively defining the beneficial thermal window and the onset of irreversible thermal damage therefore remains a major challenge.

(3) Transition from laboratory studies to engineering applications remains challenging. In real service environments, polymer friction materials must meet friction and wear performance requirements while also accounting for environmental aging, creep fatigue, impact loads, thermo-oxidative degradation, and long-term service stability. Meanwhile, the costs associated with high-performance polymer matrices, functional fillers, and complex manufacturing processes also restrict engineering applications. Therefore, achieving a balance among tribological performance, service reliability, processability, and economic cost remains a critical issue for the engineering application of polymer composites.

Based on the existing problems in this field, the following future research directions are proposed:

(1) Quantitative identification of frictional heat-generation mechanisms should be achieved by integrating mechanism specific experimental characterization with multiscale modeling. in situ Raman spectroscopy, Fourier transform infrared spectroscopy (FTIR), electron spin resonance (ESR), differential scanning calorimetry (DSC), dynamic mechanical analysis (DMA), and infrared thermography (IRT) with embedded thermocouples can be combined to track chain conformation, bond scission, radicals, heat flow, viscoelastic loss, and interfacial temperature. These data can be cross validated against MD simulations and used as inputs to FEM or COMSOL models. Bayesian inversion and machine learning can then separate the contributions of conformational, viscoelastic, plastic, interfacial shear, and tribo-chemical heat sources.

(2) Reliable criteria for beneficial and detrimental frictional heat should be established by linking material thermal transitions with interfacial evolution and operating conditions.

Just Accepted

Thermogravimetric analysis (TGA) coupled with FTIR and mass spectrometry (MS), oxidation induction time (OIT) tests, in situ Raman and ESR, and transfer film monitoring can identify critical transitions in decomposition, oxidation, and interfacial failure. These results can be integrated with Arrhenius models, time temperature superposition (TTS), the Peclet number, and the Damköhler number to describe the competition among heat generation, heat dissipation, and chemical reaction. Machine learning can further be used to construct phase diagrams for temperature, speed, load, and atmosphere. The expected outputs are thresholds such as the ratio of interfacial temperature to glass transition temperature, the ratio of interfacial temperature to melting temperature, OIT, transfer film failure, and abrupt changes in friction or wear.

(3) Engineering translation should follow a hierarchical validation route that progressively connects laboratory mechanisms with real service conditions. A multiscale validation route should be established from laboratory pin-on-disc or ring-on-block tests to full scale gear, bearing, seal, and brake bench tests, and finally to field service. Accelerated aging, creep, impact, and thermo-oxidative degradation should be included. Multiphysics simulation, machine learning surrogate models, online temperature, vibration, and triboelectric sensors, and digital twins can predict interfacial thermal states and service life. Life cycle assessment (LCA) and technoeconomic analysis (TEA) can help evaluate trade-offs among tribological performance, service reliability, processability, and cost.

Just Accepted

Funding

This work is supported by the Fundamental Research Funds for the Central Universities of China [Grant no. 3132026512].

Author contributions

Conceptualization: Dezhi Teng, Jingsi Wang; Formal analysis and investigation:Dezhi Teng, Xiaoxia Sa; Jingsi Wang; Writing - original draft preparation: Dezhi Teng; Jingsi Wang; Writing - review and editing: Jingsi Wang, Jiaqi Zhu, Pay Jun Liew; Supervision: Jingsi Wang, Pay Jun Liew.

Competing interests

The authors have no competing interests to declare that are relevant to the content of this article.

References

[1]Lv, F., Zhang, Y., Huang, C., Gao, G., Yang, P., Jiao, C., Zou, D. Mixed-lubrication analysis of polymer bearings considering elastic deformation of asperities induced by hydrodynamic pressure. *Tribol Int* **224**: 112267 (2026).

[2]Durjava, A., Mojškerc, B., Bergant, Z., Vukašinović, N. Image-based monitoring of material emissions for wear characterization of laminated polymer composite gears. *Wear* **590**: 206563 (2026).

[3]Liu, S., Dahi Taleghani, A. Engineering of polymer nanocomposites using acid-functionalized graphite nanoplatelets for high-temperature sealing purposes. *Compos B: Eng* **306**: 112772 (2025).

[4]Park, J., Song, W., Seo, H., Lee, J.J., Kwon, S.-U., Jang, H. Effect of thermoplastic polymer in brake pads on particulate matter emission: A case study with polyethylene. *Tribol Int* **173**: 107629 (2022).

[5]Feng, W., Liang, B., Li, H., Chen, J., Gao, X., Yao, D., Lu, C., Pang, X. Interconnected expanded graphite/stearic acid networks for self‐lubricating PA6 composites with excellent heat dissipation performance. *Polym Compos* **46**: 6113-6125 (2024).

[6]Heo, S.J., Kim, J., Jin, J.-U., Jeon, C., Kim, J., You, N.-H., Chae, H.G., Kim, S.G., Ku, B.-C.: Polymer-scaffold-guided graphitization for high thermal conductivity in SWCNT-derived carbon fibers. *Carbon* **254**: 121428 (2026).

Just Accepted

[7]Hou, G., Huang, X., Li, Z., Cui, Y. Wear mechanisms of carbon fiber‐reinforced resin matrix composite at extreme temperatures. *Polym Compos* **46**: S874-S888 (2025).

[8]Chen, K., Lu, Z., Wei, P., Liu, H., Wei, D., Xie, H. Study of Friction and Wear Characteristics of PEEK by Reciprocating Sliding Experiment and Temperature Dependences Simulation. *Tribol Lett* **70**: 1-16 (2022).

[9]Hale, J., Lewis, R., Carré, M.J. Rubber friction and the effect of shape. *Tribol Int* **141**: 105911 (2020).

[10] Chen, J., Zhu, J., Li, Q., Wu, H., Guo, S., Qiu, J. Constructing 3D interconnected CNTs network in PA6 composites with well-dispersed UHMWPE for excellent tribological and heat dissipation properties. *Compos B: Eng*. **246**: 110252 (2022).

[11] Li, J., Zhou, S., Liang, M., Zou, H. Fabrication of polyphenylene sulfide composites with integrated mechanical and tribological properties by synchronically adding irradiation-treated PTFE powders and short carbon fibers. *Tribol Int* **186**: 108559 (2023).

[12] Zhang, Y., He, Y., Zhou, Y., Liu, M., Wang, Y., Yuan, J., Men, X. Fabrication of RGO/CNTs/MXene 3D skeleton structure for enhancing thermal and tribological properties of epoxy composites. *Tribol Int* **179**: 108172 (2023).

[13] Gao, H., Yang, Y., Ma, L., Jia, W., Zhu, J., Li, Z., Ding, Y., Yang, S., Lu, R., Wang, J. Frictional anisotropy behavior of graphene oxide aerogel/epoxy composite and its friction mechanism exploration. *Compos B: Eng* **311**: 113191 (2026).

[14] Fan, S., Gao, C., Duan, C., Zhang, S., Zhang, P., Yu, L., Zhang, Z. Geometry effect of copper nanoparticles and nanowires on polyetheretherketone-matrix nanocomposites: Thermal conductivity, dynamic mechanical properties and wear resistance. *Compos Sci Technol* **219**: 109224 (2022).

[15] Hou, S., Wang, L., Huang, L., Wang, B., Zhang, W., Xie, J., Feng, Y., Cao, X., Zhou, A. In-situ synthesis of MXene/polyimide nanocomposite with enhanced thermal and high temperature tribological performance. *J Mater Res Technol* **36**: 8284-8295 (2025).

Just Accepted

[16] Panda, J.N., Bijwe, J., Pandey, R.K. Optimization of graphite contents in PAEK composites for best combination of performance properties. *Compos B: Eng* **174**: 106951 (2019).

[17] Meng, Z., Wang, Y., Liu, H., Yan, Y., Yan, F. Reinforced UHMWPE composites by grafting TiO2 on ATP nanofibers for improving thermal and tribological properties. *Tribol Int* **172**: 107585 (2022).

[18] Su, Y., Wang, Y., Yan, Y., Liu, H., Wang, J., Yu, Q. Structure design of 3D nickel foam in polytetrafluoroethylene interpenetrated composites with enhanced mechanical strength and thermal/electric conductivity during dynamic wear. *Tribol Int* **214**: 111346 (2026).

[19] Evans, S.M., Keogh, P.S. Efficiency and running temperature of a polymer-steel spur gear pair from slip/roll ratio fundamentals. *Tribol Int* **97**: 379-389 (2016).

[20] Černe, B., Duhovnik, J., Tavčar, J. Semi-analytical flash temperature model for thermoplastic polymer spur gears with consideration of linear thermo-mechanical material characteristics. *J Comput Des Eng* **6**: 617-628 (2019).

[21] Kalin, M., Siddiqui, M.S.N., Požar, T. Ready-to-use contact-temperature model for polymer/steel pin-on-disc contacts with some improved thermodynamic approaches. *Tribol Int* **210:** 110732 (2025).

[22] Ge, G., Wu, Y., He, Z., Wang, S., van der Heide, E. Tribological behaviour of polymer materials: mechanisms, influencing factors, and control strategies. *J Polym Res* **33**: (2026).

[23] Kennedy, F.E., Lu, Y., Baker, I. Contact temperatures and their influence on wear during pin-on-disk tribotesting. *Tribol Int* **82:** 534-542 (2015).

[24] Zhao, G., Yin, T., Song, J., Wang, G., Xue, F., Ding, Q. Continuous Heat Generation during Polymer Friction: Aperiodic Conformational Fluctuations of Molecular Chains. *ACS Appl Polym Mater* **7** 13471-13477 (2025).

[25] Kinjo, T., Yamamoto, A., Aoyagi, T., Mieda, S., Washizu, H. Layer-Resolved Frictional Mechanisms of Engineering Polymers: Contrasting Spatial Modes of Dissipation in

Just Accepted

Polyoxymethylene and Polytetrafluoroethylene. *ACS Appl Mater Interfaces* **18**: 31718-31733 (2026).

[26] Chen, D., Wu, J., Su, B., Cui, B., Teng, F., An, S., Bai, Y., Liu, X., Liu, Y., Wang, Y. Thermo-mechanical-abrasive coupling analysis of solid rubber tire under high-speed rolling. *Wear* **512-513**: 204546 (2022).

[27] Wang, L., Xiao, K., Xiang, G., Cai, J., Yang, T., Wang, J. Study on mixed thermal-visco-hyerelastic hydrodynamic lubrication performance of water-lubricated rubber bearings in deep-sea environment. *Tribol Int* **209**: 110713 (2025).

[28] Carbone, G., Putignano, C. A novel methodology to predict sliding and rolling friction of viscoelastic materials: Theory and experiments. *J Mech Phys Solids* **61**: 1822-1834 (2013).

[29] Xiang, G., Wang, L., Fillon, M., Zhou, C., Yang, T. Coupled nonlinear dynamics and mixed thermal-visco-hyperelastic hydrodynamic lubrication in water-lubricated rubber bearings. *Tribol Int* **214**: 111246 (2026).

[30] Williams, M. L., Landel, R. F., Ferry, J. D. The temperature dependence of relaxation mechanisms in amorphous polymers and other glass-forming liquids. *J Am Chem Soc* **77(14)**: 3701–3707 (1955).

[31] Lorenz, B., Persson, B. N. J., Dieluweit, S., Tada, T. Rubber friction: comparison of theory with experiment. *Eur Phys J E* **34**: 129 (2011).

[32] Shi, X., Li, W., Wang, Y., Yuan, Y., Geng, L., Zhang, Y. Frictional thermal analysis and tribological investigation of polyurethane during friction with cotton fibers. *Mater Today Commun* **48**: 113613 (2025).

[33] Laux, K.A., Jean-Fulcrand, A., Sue, H.J., Bremner, T., Wong, J.S.S. The influence of surface properties on sliding contact temperature and friction for polyetheretherketone (PEEK). *Polymer* **103:** 397-404 (2016).

[34] Deng, X., Bian, Z., Wang, Y., Guo, Z., Liu, D., Peng, J., Wu, X., Beiyuan, J., Huang, L., Xu, H., Yuan, W. Controlled PET oligomer engineering enables coordination- and covalent-strengthened

Just Accepted

aerogels for thermal insulation from waste textiles. *Chem Eng J* **530**, 173372 (2026).

[35] Blok, H. The flash temperature concept. *Wear* **6**, 483-494 (1963).

[36] Jaeger, J. Moving sources of heat and the temperature at sliding contacts. *J Proc R Soc N S W* **76**, 203-224 (1943).

[37] Archard, J.F.: The temperature of rubbing surfaces. *Wear* **2**: 438-455 (1959).

[38] Tian, X., Kennedy, F.E. Maximum and Average Flash Temperatures in Sliding Contacts. *J Tribol* **116**, 167-174 (1994).

[39] Ashby, M.F., Abulawi, J., Kong, H.S. Temperature Maps for Frictional Heating in Dry Sliding. *Tribol Trans* **34**, 577-587 (1991).

[40] Laraqi N., Alilat N., Maria, A. Baïri. Temperature and division of heat in a pin-on-disc frictional device—Exact analytical solution. *Wear* **266**: 765-770 (2008).

[41] Mu, L., Shi, Y., Feng, X., Zhu, J., Lu, X. The effect of thermal conductivity and friction coefficient on the contact temperature of polyimide composites: Experimental and finite element simulation. *Tribol Int* **53**: 45-52 (2012).

[42] Xia, Y., Yano, A., Hayashi, N., Horaguchi, N., Xie, G., Guo, D. Analysis of temperature and heat partitioning coefficient during friction between polymer and steel. *Tribol Int* **171**: 107561 (2022).

[43] Puhan, D., Wong, J.S.S. Properties of Polyetheretherketone (PEEK) transferred materials in a PEEK-steel contact. *Tribol Int* **135**: 189–199 (2019).

[44] Hernández-Álvarez, C., Martín-Hernández, P. I., Martín, I. R., Rivera-López, F., Hemmerich, H., Grzegorczyk, M., Mahlik, S., Runowski, M. Optical temperature sensor evaluation in a working gear motor: application of luminescence thermometry in industrial technology. *Adv Opt Mater* **12(17)**: 2303328 (2024).

[45] Nosko, O., Tsybrii, Y., Torrello Arias, P. G., Senatore, A. Temperature measurements at tyre tread rubber on sandpaper oscillatory sliding contacts using acicular grindable thermocouples. *Tribol*

Just Accepted

Lett **72**: 75 (2024).

[46] Nosko, O., Nagamine, T., Nosko, A. L., Romashko, A. M., Mori, H., Sato, Y. Measurement of temperature at sliding polymer surface by grindable thermocouples. *Tribol Int* **88**: 100–106 (2015).

[47] Herzog, C., Drummer, D. Test rig for the in situ measurement of the elastic tooth deflection of plastic gears. *Polymers* **15**: 1732 (2023).

[48] Lin, L., Zhao, Y., Hua, C., Schlarb, A. K. Effects of the velocity sequences on the friction and wear performance of PEEK-based materials. *Tribol Lett* **69**: 68 (2021).

[49] Černe, B., Petkovšek, M., Duhovnik, J., Tavčar, J. Thermo-mechanical modeling of polymer spur gears with experimental validation using high-speed infrared thermography. *Mech Mach Theory* **146**: 103734 (2020).

[50] Letzelter, E., Guingand, M., de Vaujany, J. P., Schlosser, P. A new experimental approach for measuring thermal behaviour in the case of nylon 6/6 cylindrical gears. *Polym Test* **29**: 1041–1051 (2010).

[51] Mao, K., Li, W., Hooke, C. J., Walton, D. Polymer gear surface thermal wear and its performance prediction. *Tribol Int* **43**: 433–439 (2010).

[52] Rowe, K. G., Bennett, A. I., Krick, B. A., Gregory Sawyer, W. In situ thermal measurements of sliding contacts. *Tribol Int* **62**: 208–214 (2013).

[53] Jean-Fulcrand, A., Masen, M. A., Bremner, T., Wong, J. S. S. High temperature tribological properties of polybenzimidazole (PBI). *Polymer* **128**: 159–168 (2017).

[54] Reparaz, J. S., Chavez-Angel, E., Wagner, M. R., Graczykowski, B., Gomis-Bresco, J., Alzina, F., Sotomayor Torres, C. M. A novel contactless technique for thermal field mapping and thermal conductivity determination: Two-Laser Raman thermometry. *Rev Sci Instrum* **85**: 034901 (2014).

[55] Maity, S., Ramanan, C., Ariese, F., MacKenzie, R. C. I., von Hauff, E. In situ visualization and quantification of electrical self-heating in conjugated polymer diodes using Raman spectroscopy. *Adv Electron Mater* **8(7)**: 2101208 (2022).

Just Accepted

[56] Okubo, H., Kagiwata, D., Nakamura, R., Takeuchi, T., Nakano, K., Tsujii, Y. Time and spatially resolved Raman spectroscopic observation for superlubricious friction interfaces of concentrated polymer brushes. *Tribol Lett* **73**: 79 (2025).

[57] Yahiaoui, M., Chabert, F., Paris, J.-Y., Nassiet, V., Denape, J. Friction, acoustic emission, and wear mechanisms of a PEKK polymer. *Tribol Int* **132**: 154–164 (2019).

[58] Guo, Y., M. Fevzi Ozaydin, Wang, D., Liang, H. Friction heating and effect on tribological properties of soft polyvinyl chloride sliding against steel. *Eur Polym J* **106**: 85–91 (2018).

[59] Saha, B., Toh, W. Q., Liu, E., Tor, S. B., Lee, J. A study on frictional behavior of PMMA against FDTS coated silicon as a function of load, velocity and temperature. *Tribol Int* **102**: 44–51 (2016).

[60] Zeng, H., Maeda, N., Chen, N., Tirrell, M., Israelachvili, J. Adhesion and friction of polystyrene surfaces around Tg. *Macromolecules* **39(6)**: 2350–2363 (2006).

[61] Kershah, T., Looijmans, S. F. S. P., Anderson, P. D., van Breemen, L. C. A. Temperature dependent two-body abrasive wear of polycarbonate surfaces. *Wear* **440–441**: 203089 (2019).

[62] Xian, G., Zhang, Z. Sliding wear of polyetherimide matrix composites: I. Influence of short carbon fibre reinforcement. *Wear* **258(5–6)**: 776–782 (2005)

[63] Wu, Y., Zeng, M., Xu, Q., Hou, S., Jin, H., Fan, L. Effects of glass-to-rubber transition of thermosetting resin matrix on the friction and wear properties of friction materials. *Tribol Int* **54**: 51–57 (2012).

[64] Wu, Y., Zeng, M., Jin, H., Xu, Q., Lu, L., Wang, J., Hou, S. Effects of glass-to-rubber transition on the friction properties of ZrO_2 reinforced polybenzoxazine nanocomposites. *Tribol Lett* **47**: 389–398 (2012).

[65] Pinedo, B., Hadfield, M., Tzanakis, I., Conte, M., Anand, M. Thermal analysis and tribological investigation on TPU and NBR elastomers applied to sealing applications. *Tribol Int* **127**: 24–36 (2018).

Just Accepted

[66] Uetz, H., Richter, K., Wiedemeyer, J. System temperature and tribological behaviour of polymer-metal sliding couples in pin-on-disc model testing. *Wear* **88**: 103–114 (1983).

[67] Dyson, C. J., Priest, M., Fox, M. F., Hopkins, B. The tribological behaviour of carbon fibre reinforced polyaryletherketones (PAEKs) through their glass transitions. *Proc Inst Mech Eng Part J: J Eng Tribol* **230(10)**: 1183–1196 (2016).

[68] Puhan, D., Jiang, S., Wong, J. S. S. Effect of carbon fiber inclusions on polymeric transfer film formation on steel. *Compos Sci Technol* **217**: 109084 (2022).

[69] Dong, F., Hou, G., Cao, F., Yan, F., Liu, L., Wang, J. The lubricity and reinforcement of carbon fibers in polyimide at high temperatures. *Tribol Int* **101**: 291–300 (2016).

[70] Li, H., Wang, L., Li, L., Li, H., Dai, Y., Hu, Q., Zhou, A., Liu, X. 2D Mo2CTx Reinforced Polyimide Nanocomposites for Enhancement of Surface Tribological Performance at Elevated Temperatures. *Adv Mater Interfaces* **10**: (2023).

[71] Chen, J., Zhu, J., Pan, Y., Wu, H., Guo, S., Qiu, J. Fabrication of wear-resistant PA6 composites with superior thermal conductivity and mechanical properties via constructing highly oriented hybrid network of SiC-packed BN platelets. *J Mater Sci Technol* **146**: 200–210 (2023).

[72] Wu, F., Chen, H., Fang, H., Wu, Y., Fang, Y., Lin, H. Ultra-low wear performance of PEKK composites synergistically reinforced with short carbon fibers and PTFE. *Tribol Int* **216**: 111520 (2026).

[73] Shi, Y., Bai, Y., Lei, Y., Zhang, H., Zhou, S., Zou, H., Liang, M., Chen, Y. Simultaneously enhanced heat dissipation and tribological properties of polyphenylene sulfide-based composites via constructing segregated network structure. *J Mater Sci Technol* **99**: 239–250 (2022).

[74] He, Y., Zhang, Z., Wang, Y., Liu, M., Yuan, J., Li, P., Yang, M., Liu, W. Inspired with fish scale to manufacture biomimetic MXene derivative for the reinforcement on tribological and mechanical properties of PPS fabric/phenolic composites. *Tribol Int* **179**: 108136 (2023).

[75] Shen, F., Ke, L.-L. A comparative study on fretting wear and frictional heating behavior of

Just Accepted

PEEK composites for artificial joint applications. *Polym Test* **109**: 107552 (2022).

[76] Boubakri, A., Elleuch, K., Guermazi, N., Ayedi, H.F.: Investigations on hygrothermal aging of thermoplastic polyurethane material. *Mater Des* **30**: 3958–3965 (2009).

[77] Ahmadijokani, F., Shojaei, A., Dordanihaghighi, S., Jafarpour, E., Mohammadi, S., Arjmand, M. Effects of hybrid carbon-aramid fiber on performance of non-asbestos organic brake friction composites. *Wear* **452-453**: 203280 (2020).

[78] Zhang, Y., Si, C., Zhang, Z., Li, L., Fan, X., Zhu, M. Hierarchical design of microcapsules-based epoxy resin coating enhanced with Ti3C2Tx for improving thermal, tribological, anti-corrosive performance. *Carbon* **228**: 119379 (2024).

[79] Jiang, Y., Chen, L., Xiao, C., Zhou, N., Qing, T., Qian, L. Friction and Wear Behaviors of Steel Ball Against Polyimide-PTFE Composite Under Rolling-Sliding Motion. *Tribol Lett* **69**: (2021).

[80] Teng, D., Wang, J., Sa, X., Zhao, T., Zhu, J.: Comparative study of tribological behaviors of compression molded polyimide under varying load conditions. *Wear* 582-583, 206359 (2025).

[81] Qi, H., Zhang, G., Zheng, Z., Yu, J., Hu, C. Tribological properties of polyimide composites reinforced with fibers rubbing against Al2O3. *Friction* **9**: 301–314 (2020).

[82] Zhang, J., Zhang, L., Du, C., Feng, Y., Wan, Y., Li, X., Yu, T., Wang, D., Zhou, F. Reversal mechanism of triboelectrification in steel-polymer friction interface for in-situ monitoring of transfer films. *Nano Energy* **120**: 109139 (2024).

[83] Zhang, N., Qu, C., Li, S., Wang, C., Xu, M., Yang, Z., Zhang, X., Wang, T., Wang, Q. Significantly enhanced tribology and thermal management by dual‐network graphene/epoxy composites. *Tribol Int* **164**: 107239 (2021).

[84] Su, Y., Wang, Y., Liu, H., Yan, F. Tribological enhancement of continuous polytetrafluoroethylene composites interpenetrated by a 3D nickel network and their frictional heat transfer mechanism. *Friction* **13:** 9440948 (2025).

[85] Bahadur, S. The development of transfer layers and their role in polymer tribology. *Wear*

Just Accepted

245(1–2): 92–99 (2000).

[86] Ye, J., Khare, H. S., Burris, D. L. Transfer film evolution and its role in promoting ultra-low wear of a PTFE nanocomposite. *Wear* **297(1–2)**: 1095–1102 (2013).

[87] White, J. R., Shyichuk, A. V. Macromolecular scission and crosslinking rate changes during polyolefin photo-oxidation. *Polym Degrad Stab* **92(7)**: 1161–1168 (2007).

[88] Fox, T. G., Flory, P. J. Second-order transition temperatures and related properties of polystyrene. I. Influence of molecular weight. *J Appl Phys* **21**: 581–591 (1950).

[89] Lu, X. Y., Jiang, B. Z. Glass transition temperature and molecular parameters of polymer. *Polymer* **32(3)**: 471–478 (1991).

[90] Kosbe, P., Patil, P., Manickam, M., Ramamurthy, G. Effect of hexagonal boron nitride (h-BN) inclusion on thermal characteristics of disc brake friction composites. *Diam Relat Mater* **107**: 107895 (2020).

[91] Wang, B., Fu, Q., Liu, Y., Yin, T., Fu, Y. The synergy effect in tribological performance of paper-based composites by MWCNT and GNPs. *Tribol Int* **123**: 200–208 (2018).

[92] Yilmaz, M., Yilmaz, N.F., Gungor, A. Wear and thermal coupled comparative analysis of additively manufactured and machined polymer gears. *Wear* **556-557**, 205525 (2024).

[93] Saikko, V., Morad, O., Viitala, R. Effect of temperature on UHMWPE and VEXLPE friction and wear against CoCr in noncyclic tests. *Wear* **490-491**: 204190 (2022).

[94] Min, C., Su, Y., Yu, H., Liang, H., Siddique, A., Xu, Z. Constructing the fluorine-containing structures for excellent tribological properties of degradable Poly(hexahydrotriazine)s. *Polymer* **333**, 128691 (2025).

[95] Bao, Q., Li, Y., Wang, N., Cheng, S., Feng, J., Wang, B., Yang, F., Li, W., Li, N., Jian, X. Fluorinated Polyphthalazine Ether Ketone Polymers with Self-Lubricating Function: Experiments and Molecular Dynamics Simulations. *ACS Appl Polym Mater* **7**: 1863–1874 (2025).

[96] Liu, G., Niu, W., Yao, Y., Fan, Y., Zhou, H., Xu, X., Li, H., Zhu, M. Low friction and wear of

Just Accepted

polycaprolactone/epoxy coatings driven by solid-liquid phase change. *Tribol Int* **204**, 110550 (2025).

[97] He, Y., Zhang, Z., Yang, M., Liao, C., Yuan, J., Li, P., Liu, W. MXene decorated hierarchical phase change microcapsules to strengthen the tribological properties of PPS/PTFE fabric composites. *Tribol Int* **199**: 110038 (2024).

[98] Chen, J., Feng, W., Li, H., Yao, D., Gao, X., Lu, C., Pang, X. Synergistic moisture-driven lubrication and frictional heat dissipation in porous LiCl/UPR composites. *Tribol Int* **211**: 110917 (2025).

[99] Islam, A., Pandey, A.K., R. Saidur, Belqasem Aljafari, Tyagi, V.V. Advancements in foam-based phase change materials: Unveiling leakage control, enhanced thermal conductivity, and promising applications. *J Energy Storage* **74**: 109380–109380 (2023).

[100] Li, Y., Cai, T., Li, Y., Jiang, Z., He, F., Chen, Z., Ali, H. M., Shehzad, N., Waqas, A., Yang, W. Pn@MF@SiO_2 double-shelled phase change microcapsules with high latent heat and low leakage rate. *ChemistrySelect* **9(5)**: e202303322 (2024).

[101] Chen, Y., Lu, X., Liu, Z., Xiao, W., Song, L., Lang, L., Li, H., Zhan, X., Gao, F., Zhang, Q. Polysiloxane-modified PMMA-shell phase change microcapsules for thermal management fabrics. *Macromol Rapid Commun*. **46**: e2400942 (2025).

[102] Chang, S., Zhang, L., Li, X., Liu, B., Meng, Y., Hu, H. Experimental study of novel paraffin-fatty acid eutectic mixtures for thermal management of electronic devices. *J Energy Storage* **84**: 110846 (2024).

[103] Han, C., Zhang, M., Gu, H., Huang, A., Zhang, J., Tan, C., Guo, C. Preparation of thermal energy storage microcapsule with double-layer ceramic shell possessing sponge effect to improve the thermal cycling performance. *Ceram Int* **50(6)**: 9420–9426 (2024).

[104] Prajapati, S.K., Gnanamoorthy, R. Effect of the infill percentage of 3D printed Polyetheretherketone under the dry sliding condition. *J Manuf Process* **131**, 2073–2081 (2024).

[105] Padhan, M., Marathe, U., Bijwe, J. A complex interdependence of thermal conductivity and

Just Accepted

lubricity of two solid lubricants to control the tribo-performance of PAEK based composites. *Wear* **458-459**: 203406 (2020).

[106] Lin, L., Pei, X., Bennewitz, R., Schlarb, A.K. Tribological Response of PEEK to Temperature Induced by Frictional and External Heating. *Tribol Lett* **67**: (2019).

[107] Tarasov, S.Yu., Buslovich, D.G., Panin, S.V., Savchenko, N.L., Kornienko, L.A., Filatov, E.Yu., Moskvichev, E.N. Structure and tribological behavior of a polyetherimide/polytetrafluoroethylene matrix filled with negative thermal expansion zirconium tungstate particles. *Wear* **558-559**: 205567 (2024).

[108] Sun, W., Chen, T., Chen, T., Liu, X., Ye, J. Shear localization in ultralow wear of PEEK/UPE composites. *Compos Pt A Appl Sci Manuf* **187**: 108484 (2024).

[109] Qi, H., Li, G., Zhang, G., Liu, G., Yu, J., Zhang, L. Distinct tribological behaviors of polyimide composites when rubbing against various metals. *Tribol Int* **146**: 106254–106254 (2020).

[110] Cheng, P., Wang, R., Hu, Z., Liu, C., Luo, Y., Fei, J., Qi, L. Enhancing high-temperature tribological properties of graphite-modified CFRP composites through interfacial engineering with in situ formed metal oxides. *Carbon* **256**, 121564 (2026).

[111] Zhu, Y., Li, H., Fei, J., Li, C., Ma, S., Cai, X., Li, B. Effect of modified nano boron nitride on tribological performance of resin-based friction material paired with copper dual disk. *Tribol Int* **168:** 107429 (2022).

[112] Zhao, Y., Zhang, S., Yu, X., Luo, C., Wei, M., Luo, D., Bai, C. h-BN bulk-to-nanosheet in-situ achieved in polyurea for boosting its thermal stability, friction, and corrosion resistance. Co*lloids Surf A***736**: 139687 (2026).

[113] Fang, Q., He, X., Wu, X., Wang, K., Luo, H., Liu, P., Yan, H., Li, C., Tu, C., Liu, Y. Enhancing high-temperature oxidation resistance and wear performance of graphite via pitch-coated h-BN. *Tribol Int* **221**: 111985 (2026).

[114] Zhang, P., Wei, D., Ding, X., Zhang, L., Qu, X. The deteriorated tribological and noise

Just Accepted

performances of copper-based brake pads induced by the increased content of flake graphite. *Eng Fail Anal* **167**: 109033 (2025).

[115] Cen, J., Li, S., Chen, K., Zhang, D. Synergistic friction and wear reduction in PEEK/PTFE composites through P-MoS2 and K-BN-OH integration. *Tribol Int* **220**: 111925 (2026).

[116] Hou, W., Xi, G., Yang, S., Wang, J., Li, Z., Han, M., Hou, K. PVDF encapsulation: An edge passivation strategy for suppressing native oxidation and tribo-oxidation of molybdenum disulfide. *Tribol Int* **220**: 111970 (2026).

[117] Feng, Y., Wang, L., Li, Z., Li, P., Huang, L., Cao, X., Hu, Q., Zhou, A., Liu, X. Fabrication and performance investigation of MXene reinforced aramid fiber/phenolic resin multifunctional friction material. *Colloids Surf A* **736**: 139592 (2026).

[118] He, G., Zhu, C., Shi, Y., Yu, Y., Wu, Y., Bao, M., Xu, H., Chizhik, S., Liu, X. MXene topological metamaterials enable thermally managed, wear-resistant self-lubricating fabric composites. *Tribol Int* **219**: 111858 (2026).

[119] He, Y., Zhang, Z., Yang, M., Liu, M., Liao, C., Li, P., Jiang, W., Yuan, J., Liu, W. Construction of 3D structured MXene-h-BN hybrid via thiol-ene click chemistry to enhance thermal and tribological properties of fabric composites. *Tribol Int* **193**: 109341 (2024).

[120] Yu, K., Ren, J., Liao, W., Hu, B., Bai, C., Li, Z., Zhang, X., Muhammad Chhattal, Li, N., Qiang, L. Maintaining the 2D Structure of MXene via Self‐Assembled Monolayers for Efficient Lubrication in High Humidity. *Small* **20**: e2402143 (2024).

[121] Fu, L., Fu, B., Zhou, M., Du, S., Zhang, Y., Shan, Q., Hua, L., Ding, Z., Zhang, G. Study on metal nanoparticles-PDA interface modification and its effect on the tribology behavior of PTFE self-lubricating coating materials. *Appl Surf Sci*. **693**: 162839 (2025).

[122] Zhang, K., Lin, Z., Ma, S., Pan, S., Chen, W., Wang, D., Chen, C., Zhao, X. Silver with tribo-chemistry facilitation synergized with graphite particles for enhancing the tribo-performance of PEEK composites. *Compos Part A Appl* **187**: 108456 (2024).

Just Accepted

[123] Li, M., Liu, N., Li, Q. A novel core-shell epoxy high performance composite: Self-lubricating, heat-resistant and self-repairing. *Prog Org Coat* **129**: 217–228 (2019).

[124] Jia, Q., Yin, H., Luo, H., Feng, L., Li, X., Cui, Y., Li, Z., Li, H. Regulation of low-friction lubrication properties in polyetheretherketone composites based on self-lubricating core-shell microcapsules. *Tribol Int* **220**: 111946–111946 (2026).

[125] Liu, H., Yang, Z., Qi, H., Wang, T., Wang, Q. Engineering intermolecular dynamic hydrogen bond interaction to regulate the tribology behaviors of shape memory polyimide. *Chem Eng J* **523**: 168441 (2025).

[126] Liao, C., Zhang, Z., He, Y., Yuan, J., Yang, M., Li, P., Jiang, W., Liang, Y., Liu, W. Bioinspired Antiwear Poly(urea‐imide) Composites: Influence of Tribology on Polymer Crystal Structure. *Small* **21**: (2025).

[127] Wu, Y., Yu, Z., Liu, X. Tribological performance of in-situ epoxy composites filled with micro-sized ZrB 2 particles. *Compos Part B: Eng* **123**: 148–153 (2017).

[128] He, L., Zhang, J., Zheng, Y., Liu, S., Liu, X., Tong, L. Boosting thermal conductivity and tribological performance of polyarylene ether nitrile synergistically by fabricating SiCws-BNNS multidimensional networks. *Compos Part A Appl* **194**: 108888 (2025).

[129] Jiang, T., Wang, Y., Xiang, L., Tang, B., Shi, S., Jiang, C., Li, R., Li, Y., Yu, W., Yu, W., Wu, X., Li, W., Zhao, Y., Sun, K., Fan, R., Yu, J. Synthesis of Ni-diamond hybrid reinforced carbon fiber/epoxy thermally conductive composites with “Rod-on-particle microstructure” via composite electrodeposition. *Compos Sci Technol* **271**: 111351 (2025).

[130] Teng, D., Wang, J., Sa, X., Zhu, J. Effects of milled carbon fiber size and content on mechanical, thermal and tribological performance of polyimide composites. *Compos Commun* **65**: 102843 (2026).

[131] Li, L., Jiang, H., Luo, Y., Wu, H., Zhao, Q., Yang, X., Li, C., Yi, J., Liu, Y. A study of the friction and thermal properties of epoxy composites synergistically reinforced by open-celled Cu

Just Accepted

foams and carboxylated CNTs. *Diam Relat Mater* **151:** 111791 (2025).

[132] Zhang, Y., He, Y., Zhou, Y., Ma, W., Yuan, J., Men, X. Investigation of the thermal and tribological properties of epoxy composite reinforced with aramid nanofiber/OMMT hybrid aerogel. *Appl Surf Sci* **654**: 159441 (2024).

[133] Zhou, Y., Zhang, Y., Wang, J., He, Y., Yuan, J., Men, X. Well-aligned MXene@MoS2/Carbon nanofiber aerogels reinforced epoxy composites with splendid thermal and tribological performance. *Carbon* **213**: 118222 (2023).

[134] Zhou, Y., Zhang, Y., Liu, M., Wang, Y., Yuan, J., Men, X. Synergistically assembled RGO/Si3N4 whiskers hybrid aerogels to endow epoxy composites with excellent thermal and tribological performance. *Friction* **11**: 2091–2106 (2023).

[135] Ma, X., Wang, W., Qi, X., Yang, J., Lei, Y., Wang, Y. Highly thermally conductive epoxy composites with anti-friction performance achieved by carbon nanofibers assisted graphene nanoplatelets assembly. *Eur Polym J* **151**: 110443 (2021).

[136] Zhang, Y., Bai, T.: Influence of graphene orientation on tribological properties of organic composite coatings from the perspective of energy transfer using molecular dynamics. *Tribol Int* **193**: 109368 (2024).

[137] Nan, C.-W., Liu, G., Lin, Y., Li, M. Interface effect on thermal conductivity of carbon nanotube composites. *Appl Phys Lett* **85**: 3549 (2004).

[138] Hasselman, D.P.H., Johnson, L.F. Effective Thermal Conductivity of Composites with Interfacial Thermal Barrier Resistance. *J Compos Mater* **21**: 508–515 (1987).

[139] Luo, T., Lloyd, J.R. Enhancement of Thermal Energy Transport Across Graphene/Graphite and Polymer Interfaces: A Molecular Dynamics Study. *Adv Funct Mater* **22**: 2495-2502 (2012).

[140] Chu, K., Jia, C., Li, W.: Effective thermal conductivity of graphene-based composites. *Appl Phys Lett* **101**: (2012).

[141] Macedo, F., Ferreira, J. A. Thermal contact resistance evaluation in polymer-based carbon

Just Accepted

fiber composites. *Rev Sci Instrum* **74(1)**: 828–830 (2003).

[142] Shen, X., Wang, Z., Wu, Y., Liu, X., He, Y.-B., Kim, J.-K. Multilayer graphene enables higher efficiency in improving thermal conductivities of graphene/epoxy composites. *Nano Lett* **16(6)**: 3585–3593 (2016).

[143] Sarikhani, N., Arabshahi, Z. S., Saberi, A. A., Moshfegh, A. Z. Unified modeling and experimental realization of electrical and thermal percolation in polymer composites. *Appl Phys Rev* **9**: 041403 (2022).

[144] Fei, X., He, W., Huang, W., Li, S., Hu, E. Tribological behaviors of onion-like carbon/waterborne polyurethane composite coatings with laser surface texturing. *Appl Surf Sci* **709**: 163849 (2025).

[145] Xiang, P., Cao, J., Long, Q., Wang, S., Wu, J., Abbas, Z. Tribological properties of PTFE/PI-PAI composite coatings filled by GO/ ZrO2 on the surfaces of different micro-textures. *Colloids Surf A* **686**: 133412 (2024).

[146] Qiu, Y., Jia, X., Shan, Z., Wang, D., Yang, J., Wang, Z., Song, H. Construction of biomimetic textures and modification of self-lubrication mechanisms on the surface of sulfonated polyether ether ketone films. *J Mater Sci* **59**: 16932–16946 (2024).

[147] Shan, Z., Jia, X., Wang, D., Yang, J., Wang, Z., Song, H. Self-Lubrication Mechanism of Surface-Textured Polymer-Matrix Composites under the Induction of Frictional Stress. *Langmuir* **40**: 18314−18323 (2024).



Just Accepted

Dezhi Teng He obtained his M. S. degrees from Dalian Maritime university (China, 2023). He is currently a PhD student at the school of marine engineering, Dalian Maritime University, China. His current research focuses on marine engine tribology and polymer tribology.



Jingsi WANG She received her B.S. degree from Dalian University of Technology (China, 2011) and her Ph.D. degree from Tohoku University (Japan, 2016). Her research interests primarily focus on marine engine tribology and surface/interface technology as well as advanced manufacturing technology. Specific topics include surface strengthening and finishing processes, design and fabrication of functional surfaces with friction-reducing and drag-reducing properties, and the coupled issues of friction, wear, corrosion, and lubrication at interfaces.

Just Accepted